Cell Reports

Article

A targeted single mutation in influenza A virus universal epitope transforms immunogenicity and protective immunity via CD4+ T cell activation

Graphical abstract

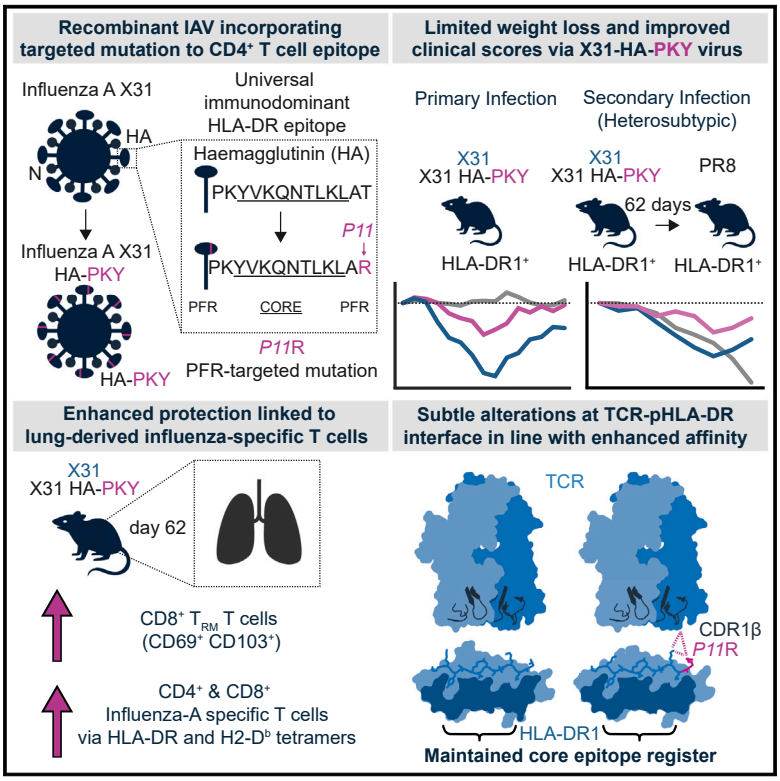

Highlights

- Modifying CD4+ T cell epitope of influenza HA transforms immunogenicity and long-term immunity
- Modified HA also induces increased CD8+ T cells to influenza NP in HLA-DR1+ mice
- Long-term heterosubtypic protection is mediated by antigen-specific lung CD4+ and CD8+ T cells
- A single mutation of a peptide-flanking residue alters TCR-pHLA-II interface and affinity

Authors

Sarah Hulin-Curtis, James K. Geary, Bruce J. MacLachlan, ..., Wendy S. Barclay, Awen Gallimore, Andrew Godkin

Correspondence

gearyj2@cardiff.ac.uk (J.K.G.), godkinaj@cardiff.ac.uk (A.G.)

In brief

Hulin-Curtis et al. demonstrate that a single targeted mutation in an HLA-DR1-presented epitope enhances control of primary influenza infection and long-term immunity after heterosubtypic re-challenge in HLA-DR1 mice. Enhanced protection appears to be mainly mediated by lung-derived T cells.

Hulin-Curtis et al., 2024, Cell Reports *43*, 114259
June 25, 2024
https://doi.org/10.1016/j.celrep.2024.114259

CellPress

Cell Reports

CellPress
OPEN ACCESS

Article

A targeted single mutation in influenza A virus universal epitope transforms immunogenicity and protective immunity via CD4+ T cell activation

Sarah Hulin-Curtis,[1,5,6] James K. Geary,[1,6,*] Bruce J. MacLachlan,[1] Danny M. Altmann,[2] Laury Baillon,[2] David K. Cole,[1] Alex Greenshields-Watson,[1,3] Sophie J. Hesketh,[1] Ian R. Humphreys,[1] Ian M. Jones,[4] Sarah N. Lauder,[1] Georgina H. Mason,[1] Kathryn Smart,[1] D. Oliver Scourfield,[1] Jake Scott,[1] Ksenia Sukhova,[2] Richard J. Stanton,[1] Aaron Wall,[1] Pierre J. Rizkallah,[1] Wendy S. Barclay,[2] Awen Gallimore,[1,6] and Andrew Godkin[1,6,7,*]

[1]Division of Infection and Immunity/Systems Immunity University Research Institute, School of Medicine, Cardiff University, Cardiff CF14 4XN, UK

[2]Faculty of Medicine, Imperial College, Hammersmith Hospital, London W12 0NN, UK

[3]Department of Statistics, University of Oxford, Oxford OX1 3LB, UK

[4]School of Biological Sciences, University of Reading, Reading RG6 6AH, UK

[5]Present address: School of Education and Applied Sciences, University of Gloucestershire, Cheltenham, Gloucestershire GL50 4AZ, UK

[6]These authors contributed equally

[7]Lead contact

*Correspondence: gearyj2@cardiff.ac.uk (J.K.G.), godkinaj@cardiff.ac.uk (A.G.)

https://doi.org/10.1016/j.celrep.2024.114259

SUMMARY

CD4+ T cells are central to adaptive immunity. Their role in cross-protection in viral infections such as influenza and severe acute respiratory syndrome (SARS) is well documented; however, molecular rules governing T cell receptor (TCR) engagement of peptide-human leukocyte antigen (pHLA) class II are less understood. Here, we exploit an aspect of HLA class II presentation, the peptide-flanking residues (PFRs), to "tune" CD4+ T cell responses within an *in vivo* model system of influenza. Using a recombinant virus containing targeted substitutions at immunodominant HLA-DR1 epitopes, we demonstrate limited weight loss and improved clinical scores after heterosubtypic re-challenge. We observe enhanced protection linked to lung-derived influenza-specific CD4+ and CD8+ T cells prior to re-infection. Structural analysis of the ternary TCR:pHLA complex identifies that flanking amino acids influence side chains in the core 9-mer peptide, increasing TCR affinity. Augmentation of CD4+ T cell immunity is achievable with a single mutation, representing a strategy to enhance adaptive immunity that is decoupled from vaccine modality.

INTRODUCTION

The endemic seasonal respiratory pathogen influenza A virus (IAV) remains a continual threat, accounting globally for 290,000–650,000 deaths each year.[1] Many infected individuals clear the virus and recover, with helper CD4+ T cells playing a key role in generating protective immunity.[2–6] Their function in initial IAV infection is characterized by helping both the recruitment and activation of cytotoxic CD8+ T cells at mucosal sites and the production of antibodies by B cells.[4,7–12] CD4+ T cells produce anti-viral cytokines and have been shown to be directly cytotoxic to influenza-infected cells *in vitro* and *in vivo*.[13–16] Thus, they are crucially important in providing both direct and indirect anti-viral responses in the early and late stages of IAV infection.[17]

Most current influenza vaccines induce neutralizing antibodies to surface-exposed hemagglutinin (HA) and neuraminidase (NA) proteins found in subtypes of IAV such as seasonal circulating H3N2 and pandemic 2009 H1N1 influenza.[18] Virus-specific antibodies are detected 7–12 days after primary infection and correlate with protection from infection with homologous strains.[19] However, the protection they provide wanes in a population over time, exacerbated by exposure to antigenically drifted strains necessitating reformulation of annual vaccines that match HA sequences to circulating seasonal strains. Furthermore, vaccine- or infection-induced antibodies offer practically no protection against novel subtypes, which may have pandemic potential.

Vaccines generating CD4+ T cell responses to viral epitopes (even single epitopes) can provide protection from lethal infection,[20,21] although immune responses are often inadequate.[22] Therefore, the development of approaches to augment CD4+ T cell responses could represent an effective strategy for improved vaccines and offer improved protection in particularly vulnerable groups such as the elderly (reviewed in Pop-Vicas and Gravenstein[23] and Buchy and Badur[24]) or those co-infected

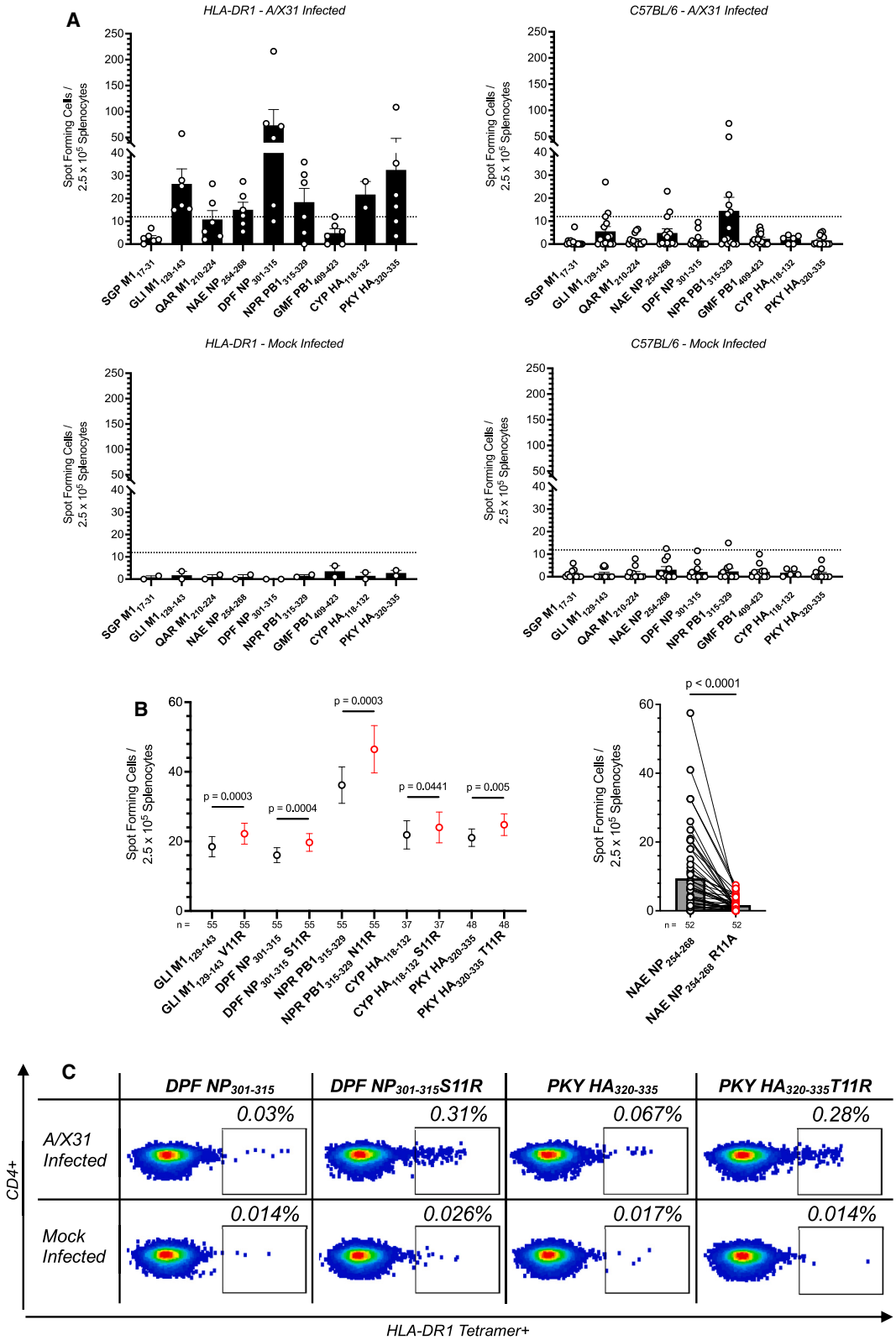

(legend on next page)

with HIV.[25,26] Furthermore, vaccines inducing cross-protective immune responses by targeting conserved B cell or T cell epitopes across different viral strains (so-called universal epitopes) provide the basis for broad protection.[27] The PKY $HA_{320-335}$ peptide can be presented by several allotypes including human leukocyte antigen (HLA)-DR1 and HLA-DR4,[28–30] thereby potentially representing a universal epitope by capture of multiple HLA alleles of the human population.

Epitopes presented by major histocompatibility complex (MHC) class II molecules contain a core nonamer (9-mer) peptide bound within the open groove of the MHC heterodimer, with key binding pockets found usually at positions (*P*s) 1, 4, 6, and 9; one or more solvent-exposed residues (*P*2, *P*3, *P*5, *P*7, and *P*8) are key to recognition by the T cell receptor (TCR). In contrast to MHC class I molecules, which largely present 9 or 10 amino acid peptides bound in a closed groove, peptides presented by MHC class II molecules are longer, due in part to the open-ended nature of the binding groove. Longer peptides extend beyond the context of the core binding nonamer, and these peptide-flanking residues (PFRs) are also recognized by the TCR and influence immunogenicity.[31,32] Peptide elution studies revealed HLA-transcending enrichment of amino acids in the PFRs, which may alter the immunogenicity of known MHC class II epitopes.[33] For instance, detailed *in vitro* molecular characterization of PFRs by substituting native residues of the IAV universal PKY $HA_{320-335}$ epitope with different residues revealed enhanced TCR:pMHC class II affinity and altered TCR repertoire selection with the positively charged Arg residue at *P*10 or *P*11.[34] The details of the altered TCR:pHLA contacts when employing an Arg-modified epitope have not yet been elucidated.

In this study, we set out to improve protection against IAV infection by manipulating $CD4^+$ T cell epitopes in a bespoke fashion to markedly alter T cell responses. We have previously described in detail a series of HLA-DR1-restricted epitopes derived from IAV, defining the core nonamer binding regions by peptide-HLA-DR1 structures.[35] Here, we generated recombinant A/X31 H3N2 IAV incorporating an Arg at *P*11 in the PFR of a known HLA-DR1-restricted epitope, which was then tested in HLA-DR1 transgenic mice. We evaluated the immunogenicity of recombinant versus wild-type (WT) IAV in these HLA-DR1 mice and measured the impact of those responses on long-term memory (>60 days) with heterosubtypic PR8 H1N1 challenge. Finally, in an attempt to understand the impact of PFR modifications at the molecular level, we generated ternary structures of TCR:pHLA-II employing both WT and *P*11R-modified epitopes.

RESULTS

Characterization of $CD4^+$ T cell responses in IAV-infected HLA-DR1 mice

In a previous study, we fine-mapped epitopes of internal IAV proteins in HLA-DR1+ human blood donors[35] and demonstrated immunodominant $CD4^+$ T cell responses to HLA-DR1-restricted epitopes in matrix protein (M1), nucleoprotein (NP), polymerase basic protein (PB-1), and HA. To establish whether we could recapitulate responses in HLA-DR1 transgenic mice,[36] we measured $CD4^+$ T cell responses to A/X31, a laboratory-adapted strain of a human seasonal flu H3N2 virus. Mice were infected with A/X31 and sacrificed 14 days later, and peptide-specific T cell responses were measured in an interferon γ (IFN-γ) ELISpot assay. As shown in Figure 1A, five of the previously described flu epitopes were recognized by splenocytes from HLA-DR1, but not C57BL/6, mice: GLI ($M1_{129-143}$), DPF ($NP_{301-315}$), NPR ($PB\text{-}1_{315-329}$), CYP ($HA_{118-132}$), and PKY ($HA_{320-335}$). No responses were observed in mock-infected mice. When HLA-DR1 mice were infected with the heterosubtypic PR8 strain of IAV (H1N1), responses to peptides derived from shared internal proteins (M1, NP, PB-1) were observed, while responses to peptides from the variable HA (H3) protein were not (Figure S1).

Immunodominant influenza-specific $CD8^+$ T cell responses in C57BL/6 mice are well characterized and play a key role in viral control.[37,38] As $CD4^+$ T cells provide help for $CD8^+$ T cells, we wished to determine whether robust influenza-specific $CD8^+$ T cell responses are observed in HLA-DR1 mice, which lack the mouse class II molecule, $I\text{-}A^b$. Following infection with A/X31, $CD8^+$ T cell responses to the immunodominant $NP_{366-374}$ and $PA_{224-233}$ and subdominant $PB1\text{-}F2_{62-70}$ $H\text{-}2D^b$-restricted epitopes were observed, implying that $CD4^+$ T cell help is provided by the HLA-DR1-restricted peptides described above (Figure S2).

Ex vivo $CD4^+$ T cell responses are enhanced with *P*11R-modified peptides

To establish whether targeted modifications of epitopes at *P*11 in the C-terminal PFR (X→R [Arg], termed *P*11R) enhance the T cell response to influenza epitopes, we restimulated splenocytes *ex vivo* from A/X31-infected HLA-DR1 mice with either WT or *P*11R-modified peptides (Table S1). Splenocytes restimulated with *P*11R-modified peptides demonstrated significantly enhanced $CD4^+$ T cell responses for each of the epitopes tested (Figure 1B, left), confirming and expanding our previous observations using human T cells that the basic residue may alter the immunogenicity of the epitope.[34] Conversely,

Figure 1. Characterization of $CD4^+$ T cell responses in IAV-infected HLA-DR1 mice

(A) *Ex vivo* IFN-γ ELISpot responses of mouse splenocytes restimulated with HLA-DR1-restricted peptides at day 14 after A/X31 primary infection (n = 6–14 mice) or mock PBS infection (n = 2–8 mice) in HLA-DR1 and C57BL/6 mice. Each symbol represents an individual mouse. Bars represent the mean values (±SEM). The dotted line represents the threshold for positive T cell response. Data are pooled from up to three independent experiments.

(B) *Ex vivo* IFN-γ ELISpot responses of mouse splenocytes restimulated with wild-type (WT) or *P*11R-modified peptide at either day 8 or 14 after A/X31 primary infection of HLA-DR1 mice (left) and abrogation of response to native arginine at *P*11 by restimulation with alanine (nonpolar residue) (right). Numbers under graphs represent total numbers of mice. Symbols (left) represent the mean values (±SEM) or each individual mouse (right). p values are from paired Student's t test. Data are pooled from seven (left) and six (right) independent experiments.

(C) Representative flow cytometry plots showing *ex vivo* frequencies (%) of $CD4^+$ HLA-DR1 tetramer+ cells from splenocytes of HLA-DR1 mice infected with A/X31 or mock-infected mice at day 14 after primary infection. Data are representative of 8 mice, showing a highly significant increase in staining with *P*11R tetramers (shown in Figure S3).

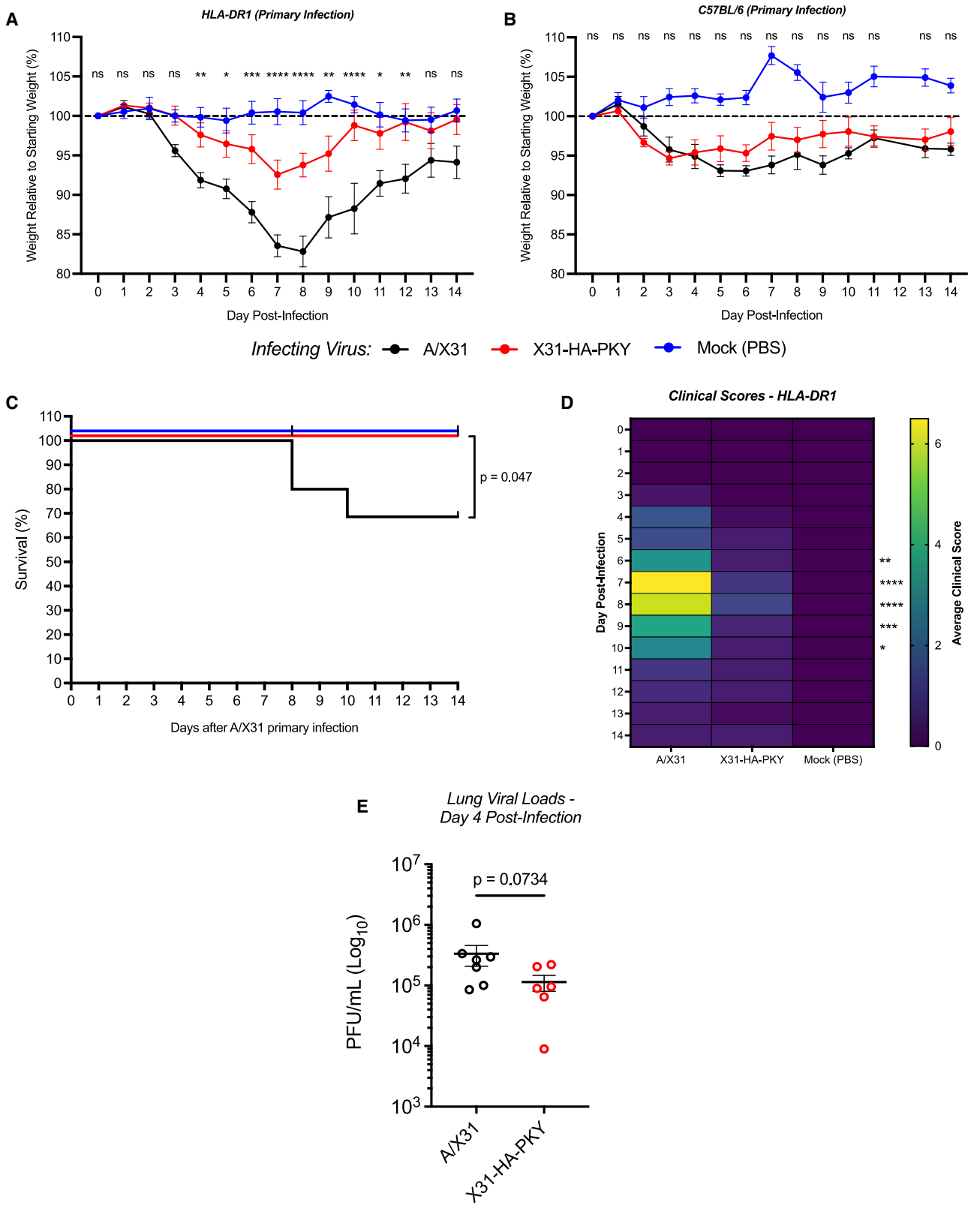

(legend on next page)

in the case of the NAE peptide ($NP_{254-268}$), substitution of the WT Arg at *P*11 to an Ala resulted in complete loss of the response, further supporting the notion that basic residues are favored at *P*11 of certain HLA-DR1-restricted epitopes (Figure 1B, right, $p < 0.0001$).

Enhanced numbers of antigen-specific cells are detected using HLA-DR1 tetramers comprising *P*11R-modified peptides

To further examine the effect of *P*11R modification on TCR:pHLA-II interactions, we made HLA multimers refolded with WT DPF $NP_{301-315}$ or PKY $HA_{320-335}$ or incorporating *P*11R-modified peptides DPF $NP_{301-315}$S11R and PKY $HA_{320-335}$T11R (peptide sequences are listed in Table S1). These reagents were used to stain splenocytes from A/X31- or mock-infected (PBS) mice (Figure 1C). We consistently observed an approximately 2-fold increase in numbers of $CD4^+$ T cells when staining with DPF $NP_{301-315}$S11R or PKY $HA_{320-335}$T11R tetramers in comparison to the WT tetramer (Figure S3). As reported previously for human T cells,[39] this most likely reflects an increased avidity of the TCR for the *P*11R-modified HLA-DR1 tetramer.

Recombinant A/X31 virus incorporating *P*11R-modified epitope causes milder disease in infected mice

To examine whether *P*11R modifications enhance the priming of $CD4^+$ T cell responses in mice, a series of recombinant A/X31 influenza viruses incorporating *P*11R modifications in HLA-DR1-restricted epitopes within the M1, NP, or HA gene segments were generated. Despite multiple attempts, we were not able to rescue recombinant viruses with the engineered substitutions in the M1 and NP genes; however, both viruses with mutations in the H3 HA were rescued (Table S2). We performed multicycle replication assays to understand whether the substitutions in HA affected virus fitness. The *in vitro* replication kinetics of X31-HA-PKY virus were almost identical to WT parental A/X31 virus (Figure S4). Hence, the variant virus X31-HA-PKY was chosen for further *in vivo* experiments. Furthermore, $HA_{320-335}$ is a well-characterized epitope that is presented by a wide range of MHC class II alleles, and therefore studying the effect of enhancing epitope presentation by engineering at *P*11 is a widely applicable strategy to potentially improving immune responses in a good proportion of the population.[40–43]

To test whether modification of this IAV epitope would impact the outcome of primary IAV infection, HLA-DR1 mice were intranasally infected with a low dose (200 plaque-forming units [PFUs]) of either A/X31- or X31-HA-PKY-modified virus or were mock infected (PBS) and bodyweight measured at the same time each day for 14 days (Figure 2A). Mice infected with X31-HA-PKY virus had markedly reduced weight loss compared to those infected with A/X31, a difference that was not seen in C57BL/6 mice (Figure 2B). This suggests that the reduced weight loss observed in X31-HA-PKY mice is directly related to the modified MHC class II epitope. Moreover, whereas approximately 20% of HLA-DR1 mice receiving A/X31 succumbed to infection, all mice infected with X31-HA-PKY survived ($p < 0.05$) (Figure 2C). The improved outcome data were reflected by significantly better clinical signs in X31-HA-PKY- compared to A/X31-infected HLA-DR1 mice, e.g., normal activity, limited weight loss, and no hunching of the back (Figure 2D; Table S3). Viral titers in the lungs of X31-HA-PKY-primed mice were reduced at day 4 post-infection (Figure 2E), implying that the response generated to X31-HA-PKY better controlled the infection when compared to that generated by A/X31 in HLA-DR1 mice. Although at day 4 after intranasal infection, T cell responses are absent in splenocytes, we measured responses in splenocytes at day 8 by both *ex vivo* ELISpot and tetramer staining and revealed an increase in both $CD4^+$ and $CD8^+$ influenza-specific T cell responses in mice infected with modified X31-HA-PKY (Figure S5).

Primary infection with X31-HA-PKY offers superior protection against heterosubtypic challenge with PR8

T cells offer immunity to IAV infection and are vital for heterosubtypic protection when serological responses are absent or inadequate (reviewed in Jansen et al.[6]). At day 63 after primary infection with X31-HA-PKY or A/X31 (H3N2), mice were challenged intranasally with 50 PFUs of the heterosubtypic virus PR8 (H1N1). PR8 shares the same internal genes of A/X31 but expresses H1 and N1 cell surface proteins, whereas A/X31 expresses distinct H3 and N2 proteins: therefore, immune responses that offer protection to the second virus are likely to be T cell driven and not antibody mediated. All mice previously exposed to IAV cleared the virus in the lungs by day 8, whereas high virus titers were measurable in previously unexposed naive mice (Figure 3A). While both X31-HA-PKY- and A/X31-primed

Figure 2. Recombinant A/X31 virus incorporating *P11*R-modified epitope causes milder disease in infected mice

(A) Bodyweights of HLA-DR1 mice at days 0–14 after primary infection with 200 PFUs of A/X31 ($n = 10$ mice), X31-HA-PKY ($n = 10$ mice), or mock infection (PBS) ($n = 7$ mice). Weights are represented as a percentage of the starting weight. Symbols represent the mean at each time point (±SEM). *p* values are from two-way ANOVA (Tukey's multiple comparisons test), representing significant differences between the mean weights of A/X31- and X31-HA-PKY-infected mice. Data are from two independent experiments.

(B) Bodyweights of C57BL/6 mice at days 0–14 after primary infection with 200 PFUs of A/X31 ($n = 5$ mice), X31-HA-PKY ($n = 5$ mice), or mock infection ($n = 5$ mice).

(C) Survival plot of HLA-DR1 mice infected with A/X31 ($n = 10$ mice), X31-HA-PKY ($n = 10$ mice), or mock infection ($n = 8$ mice). *p* value is from one-way ANOVA. Data are pooled from three independent experiments.

(D) Heatmap representing the clinical scores at days 0–14 of HLA-DR1 mice infected with 200 PFUs of A/X31 ($n = 6$ mice), X31-HA-PKY ($n = 6$ mice), or mock infection (PBS) ($n = 4$ mice). Each cell represents the mean clinical score at each time point (scale on right-hand side). The clinical scoring point system was defined as follows: appearance, 0–3; reduced activity, 0–4; weight loss, 0–6 (full scoring system is shown in Table S3). *p* values are from two-way ANOVA, representing significant differences between the mean clinical scores of A/X31- and X31-HA-PKY-infected mice.

(E) Lung viral titers (PFUs per mL – $\log_{10}$ scale) in HLA-DR1 mice infected with A/X31 ($n = 7$ mice) and X31-HA-PKY ($n = 7$ mice) at day 4 after primary infection. Each symbol represents an individual mouse. Horizontal line represents the mean (±SEM). *p* value is from Mann Whitney test. Data were generated from two independent experiments. $^*p < 0.05$, $^{**}p < 0.01$, $^{***}p < 0.001$, and $^{****}p < 0.0001$.

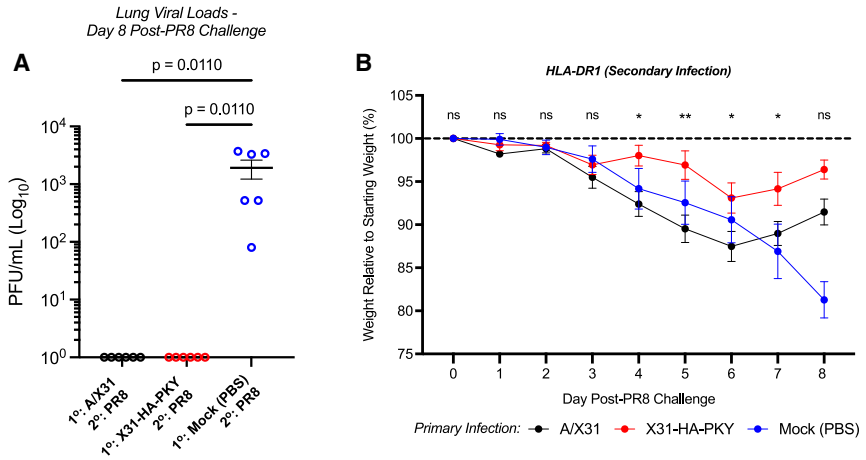

Figure 3. Primary infection with X31-HA-PKY offers superior protection against heterosubtypic challenge with PR8

(A) Lung viral titers (PFUs per mL – $\log_{10}$ scale) in HLA-DR1 mice primary (1°) infected with A/X31 (n = 6 mice), X31-HA-PKY (n = 6 mice), or mock (PBS) (n = 6 mice) at day 8 after PR8 secondary (2°) infection. Each symbol represents an individual mouse. Horizontal line represents the mean (±SEM). p value is from one-way ANOVA. Data were generated from two independent experiments.

(B) Bodyweights of HLA-DR1 mice at days 0–8 after 50 PFUs of PR8 secondary infection (primary infection: A/X31 [n = 4 mice], X31-HA-PKY [n = 5 mice], or mock infection [PBS] [n = 4 mice]). Weights are represented as a percentage of the starting weight. Symbols represent the mean at each time point (±SEM). p values are from two-way ANOVA (Tukey's multiple comparisons test), representing significant differences between the mean weights of A/X31- and X31-HA-PKY-primed mice. *$p < 0.05$ and **$p < 0.01$. Data are from two independent experiments.

mice controlled the virus, the degree of weight loss was significantly greater in mice previously infected with A/X31 compared to mice infected with X31-HA-PKY (Figure 3B). PR8-challenged, A/X31-primed mice displayed signs of listlessness and reduced activity, while those primed with X31-HA-PKY appeared completely normal (movement, socialization, etc.) despite some slight weight loss. Hence, mice infected with a bespoke virus that directly increases CD4$^+$ T cell activation by modifying a single epitope were better protected at re-challenge 2 months later with a heterosubtypic strain of influenza virus.

Memory CD4$^+$ and CD8$^+$ T cell responses are enhanced in X31-HA-PKY-primed mice

After heterosubtypic challenge with PR8, we measured serological and T cell responses 8 days after challenge. A/X31- and X31-HA-PKY-primed mice had similar levels of HA-specific antibody titers against the X31 (Figure S6A) and PR8 (Figure S6B) IAV strains. Significantly lower HA titers were observed against A/PR8 for previously naive mice (titers below the defined seroprotection threshold in half of the mice), suggesting a level of cross-reactivity with pre-existing anti-H3 antibodies in A/X31- and X31-HA-PKY-primed mice (Figure S6B).

Both A/X31- and X31-HA-PKY-primed mice demonstrated almost identical *ex vivo* CD4$^+$ and CD8$^+$ T cell responses in splenocytes measured 8 days after PR8 challenge (Figure S7). In order to identify mechanisms of protection afforded by initial X31-HA-PKY infection, immune responses were measured in previously infected mice at day 62 after primary infection but prior to the point of re-challenge in the experiment shown in Figure S7. Both *ex vivo* and cultured T cell responses from splenocytes were difficult to identify at this time point. However, this paucity of measurable splenic responses is in marked contrast to lung-derived T cells. X31-HA-PKY-primed mice demonstrated an increased level of NP$_{366\text{-}374}$-specific CD8$^+$ T cells in the lungs even at day 62 when stained *ex vivo* to the immunodominant epitope using NP$_{366\text{-}374}$ tetramers compared to those of A/X31-primed mice (Figures 4A and 4B). There was a highly significant increase in these lung-derived cells when compared to control mice.

This increased frequency of antigen-specific cells derived from the lung may reflect in part a specific subpopulation of tissue-resident memory (T_{RM}) cells. To explore this concept, mice were infected with A/X31, X31-HA-PKY, or saline control and sacrificed 62 days later. After the lungs were extensively perfused with saline, lung-derived T cells were purified and stained with a panel of MHC class I influenza-specific tetramers and the CD8$^+$ T cells phenotyped further with markers known to be associated with T_{RM} cells (CD69 and CD103). As highlighted above, there was a significant increase in influenza-specific CD8$^+$ T cells in the lung tissue of mice infected with X31-HA-PKY compared to controls, particularly compared to the immunodominant epitope NP$_{366\text{-}374}$ (Figures 4A and 4B). Further phenotyping of total CD8$^+$ T cells revealed an increased expression of either CD69$^+$ or CD69$^+$CD103$^+$, which accounted for the significant increase in CD8$^+$ T_{RM} cells in X31-HA-PKY-infected mice compared to saline controls (Figures 4C and 4D). Mice were further examined at day 62 post-primary infection time point with HLA-DR1-HA$_{320\text{-}335}$/HLA-DR1-HA$_{320\text{-}335}$T11R tetramers. Only X31-HA-PKY-infected mice had significantly higher frequencies of CD4$^+$ T cells stained with HLA-DR1-HA$_{320\text{-}335}$T11R compared to staining with HLA-DR1-HA$_{320\text{-}335}$ (Figure S8A). Furthermore, the HLA-DR1-HA$_{320\text{-}335}$T11R tetramer stained a significantly higher proportion of CD4$^+$ T cells in X31-HA-PKY-primed mice compared to A/X31- or saline-primed mice (Figure S8A). Additionally, there was a highly significant correlation between the HLA-DR1-HA$_{320\text{-}335}$T11R-specific CD4$^+$ T cell response with the NP$_{366\text{-}374}$-specific CD8$^+$ T cell response exclusively in the X31-HA-PKY-infected mice (Figure S8B). Collectively, these data demonstrate that a single change to a CD4$^+$ T cell epitope results in superior memory CD8$^+$ T cell responses, which offers protection against clinical disease with a heterosubtypic IAV.

The structures of HLA-DR1 bound to peptides HA$_{320\text{-}335}$ or the PFR-modified peptide HA$_{320\text{-}335}$-*P*11R reveal identical register binding

To understand mechanistically how *P*11R modifications may influence TCR affinity, we first solved the X-ray crystal structure of

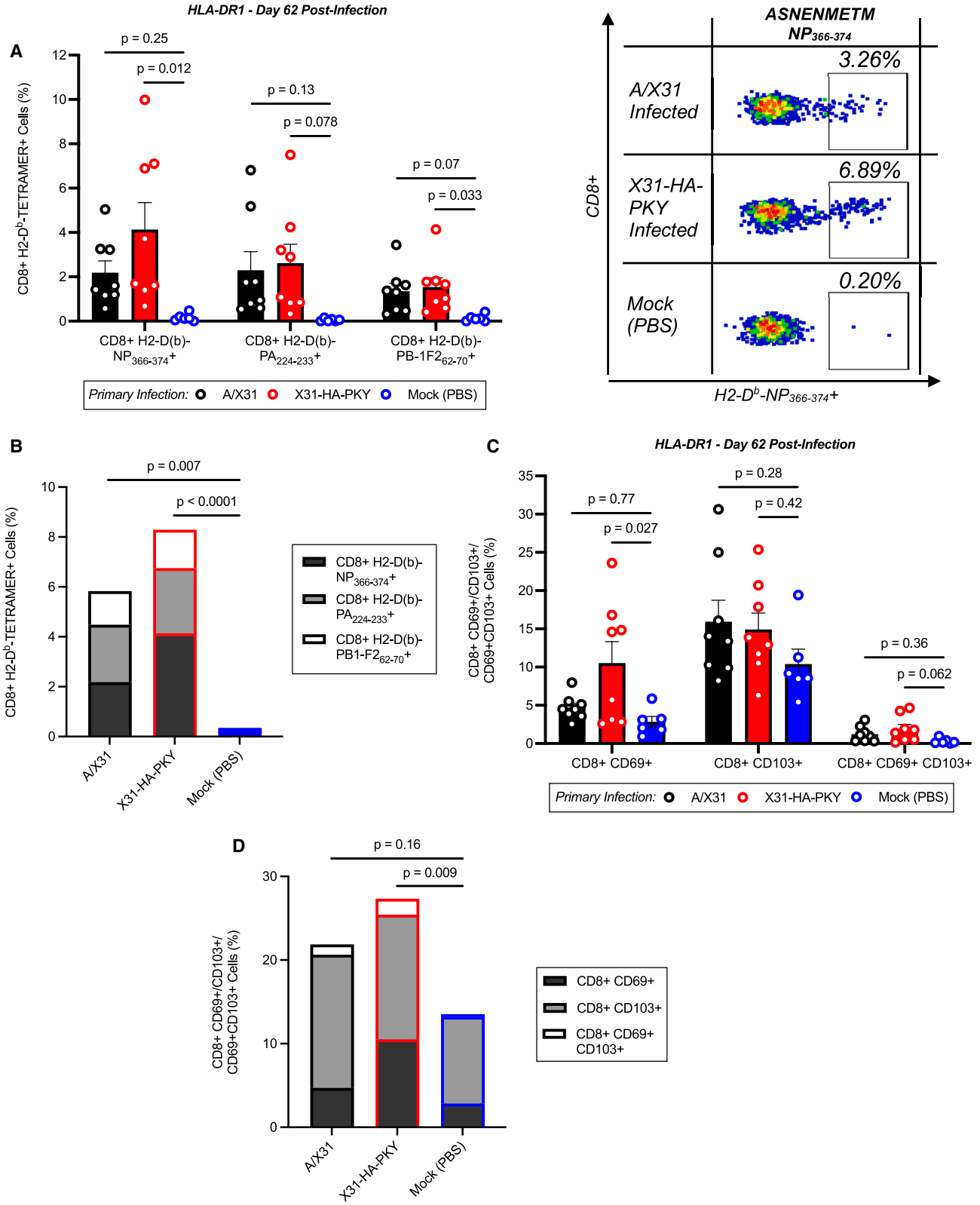

(legend on next page)

HLA-DR1 presenting the peptide $HA_{320-335}$ or variant $HA_{320-335}$-*P*11R (Figures 5A and 5B). The two crystal structures were observed in space groups *P 1 2₁ 1* and *P 2₁ 2₁ 2*, respectively, and at similar resolutions of 1.7 and 1.5 Å (data collection and refinement statistics are presented in Table S4). The overall structures of HLA-DR1-$HA_{320-335}$ and HLA-DR1- $HA_{320-335}$ *P*11R were highly similar and bound in the register seen previously.[44] The modification did not appear to alter the nature of the presented peptide; in both complexes, the C-terminal *P*11 modification (T/R) did not make contact with the HLA platform, with *P*11 (T/R) exhibiting elevated B-factors, indicative of higher mobility of atoms (*P*11T average B-factors: backbone = 59 $Å^2$, side chain = 60 $Å^2$; *P*11R average B-factors: backbone = 69 $Å^2$, side chain = 80 $Å^2$). This observation is corroborated by our previous molecular dynamics simulations indicating that PFRs are highly mobile entities.[45] Hence, the *P*11R-modified $HA_{320-335}$ epitope induced no significant changes to the peptide-HLA-DR1 complex.

The ternary structure reveals mechanisms of increased TCR affinity for $HA_{320-335}$-*P*11R via interactions with the germline-encoded VβCDR1

We found germline- and nongermline-enriched acidic amino acid-containing CDR loops in HLA-DR1-$HA_{320-335}$-specific TCR clonotyping data, presumably driven to a degree by an interaction with multiple basic Lys residues, i.e., at $P^{-}1$, *P*3, and *P*8.[35] We have also previously shown that $HA_{320-335}$ (*P*11R) modification allows a ~2-fold increase in TCR binding affinity measured by surface plasmon resonance to HLA-DR1 in a number of cloned and expressed TCRs, even though these TCRs were clones from T cells expanded on the WT $HA_{320-335}$.[34] To contextualize this finding with the observation that the *P*11R epitope drives a better outcome in the HLA-DR1 mice, the ternary crystal structure of the F11 TCR bound to HLA-DR1-$HA_{320-335}$ (*P*11R) was generated (space group *P 2₁ 2₁ 2* at 1.8 Å resolution; data collection and refinement statistics are shown in Table S4) and compared to our previously solved[35] equivalent unmodified structure (Figures 5C–5H).

The overall mode of binding of F11 to the two peptides was very similar, demonstrated by the virtually identical binding crossing angles and CDR loop positioning (Figure 5D) and in keeping with previously described ternary pMHC class II:TCR complexes.[46] The CDR1β loop of F11 binds over the C-terminal PFR, proximal to *P*11 (Figure 5D). The F11 CDR1β loop is encoded by the germline TRBV24-1 and contains negatively charged Asp at IMGT *P*37 (KGH**D**RM) and positively charged Lys, His, and Arg at *P*27, *P*29, and *P*38 (**K**G**H**D**R**M) (Figure 5E). While in the unmodified structure, the CDR1β loop did not contact *P*11T, the elongated *P*11R reached the CDR1β loop of F11 and directly contacted the carboxyl backbone of Lys27, generating two weak H-bonds (3.6 and 3.8 Å) (Figure 5F). Further, the *P*11R side chain also formed a water bridge to the CDR1β backbone (Lys27 and Gly28 carbonyls). Furthermore, the *P*11R also pushed the *P*8K toward the acidic Asp37 of CDR1β, shortening the salt bridge from 3.8 Å in the WT *P*11T to 3.3 Å in *P*11R, potentially increasing the enthalpy via this closer contact. As in the binary structures, the *P*11R atoms refined with high B-factors (*P*11T average B-factors: backbone = 72 $Å^2$, side chain = 73 $Å^2$; *P*11R average B-factors: backbone = 81 $Å^2$, side chain = 81 $Å^2$) corresponded with weak electron density about the Arg side chain. However, clear additional density at the proximal *P*8 was observed (compare Figures 5G and 5H): the altered positioning of *P*8K induced by *P*11R was supported by strong electron density in both refined maps and calculated omit maps.

In summary, these subtle changes induced by $HA_{320-335}$ *P*11R modification (epitope nonspecific via *P*11R contacts to backbone CDR1β and epitope-specific via knockon effects on *P*8K) is sufficient to cause enhanced TCR binding affinity, which in turn impacts T cell function and, in the whole animal, protective immunity. Although we have not yet generated further ternary structures, we have explored series of *P*11 substitutions on several $CD4^+$ T cell clones,[34] and the frequent favoring of basic resides at *P*11 suggests that similar mechanisms come into play, generating a subtle increase in bonds and affinity between the TCR and pHLA-II.

DISCUSSION

Generating effective immunity to influenza in high-risk groups such as the elderly remains a challenge. Both T cells and antibodies have roles in protection after infection, and a key coordinator of an overall effective response is the helper $CD4^+$ T cell.[2–12] We employed a strategy to boost the $CD4^+$ T cell response by targeting known epitopes within the intact virus. The $CD4^+$ T cell recognizes epitopes of approximately 15 amino acids in length presented by MHC class II molecules processed from viral proteins by antigen-presenting cells (APCs). The core central nonamer (*P*1–*P*9) binds with a specific motif to the particular MHC class II subtype, but previous work has shown the nonbound PFRs can be altered to increase T cell activation without altering specificity.[31–34,39,47–49] Having clearly defined the core,

Figure 4. Memory $CD4^+$ and $CD8^+$ T cell responses are enhanced in X31-HA-PKY-primed mice

(A) Left: the percentage of H2-D^b tetramer+ cells from total $CD8^+$ T cells for the immunodominant epitope $NP_{366-374}$ and subdominant epitopes $PA_{224-233}$ and PB1-$F2_{62-70}$ in the lung tissue of HLA-DR1 mice at day 62 after primary infection with A/X31 (*n* = 8 mice), X31-HA-PKY (*n* = 8 mice), or mock (PBS) (*n* = 6 mice). Each symbol represents an individual mouse. Bars represent the mean (±SEM). *p* values are from one-way ANOVA. Data are from two independent experiments. Right: representative flow cytometry plots showing *ex vivo* frequencies (%) of $CD8^+$ H2-D^b-$NP_{366-374}$+ cells in the lung tissue of mice at day 62 after primary infection.

(B) Summary of (A) showing the cumulative mean proportion (%) of $CD8^+$ T cells that were stained with H2-D^b-$NP_{366-374}$, H2-D^b-$PA_{224-233}$, and H2-D^b-PB1-$F2_{62-70}$ MHC class I tetramers. *p* values are from one-way ANOVA.

(C) The percentage of $CD8^+$ T cells expressing markers associated with tissue residency (CD69 and CD103) in the lung tissue of HLA-DR1 mice at day 62 after primary infection with A/X31 (*n* = 8 mice), X31-HA-PKY (*n* = 8 mice), or mock (PBS) (*n* = 6 mice). Each symbol represents an individual mouse. Bars represent the mean (±SEM). *p* values are from one-way ANOVA. Data are from two independent experiments.

(D) Summary of (C) showing the cumulative mean proportion (%) of $CD8^+$ T cells that were stained with CD69 and CD103. *p* values are from two-way ANOVA.

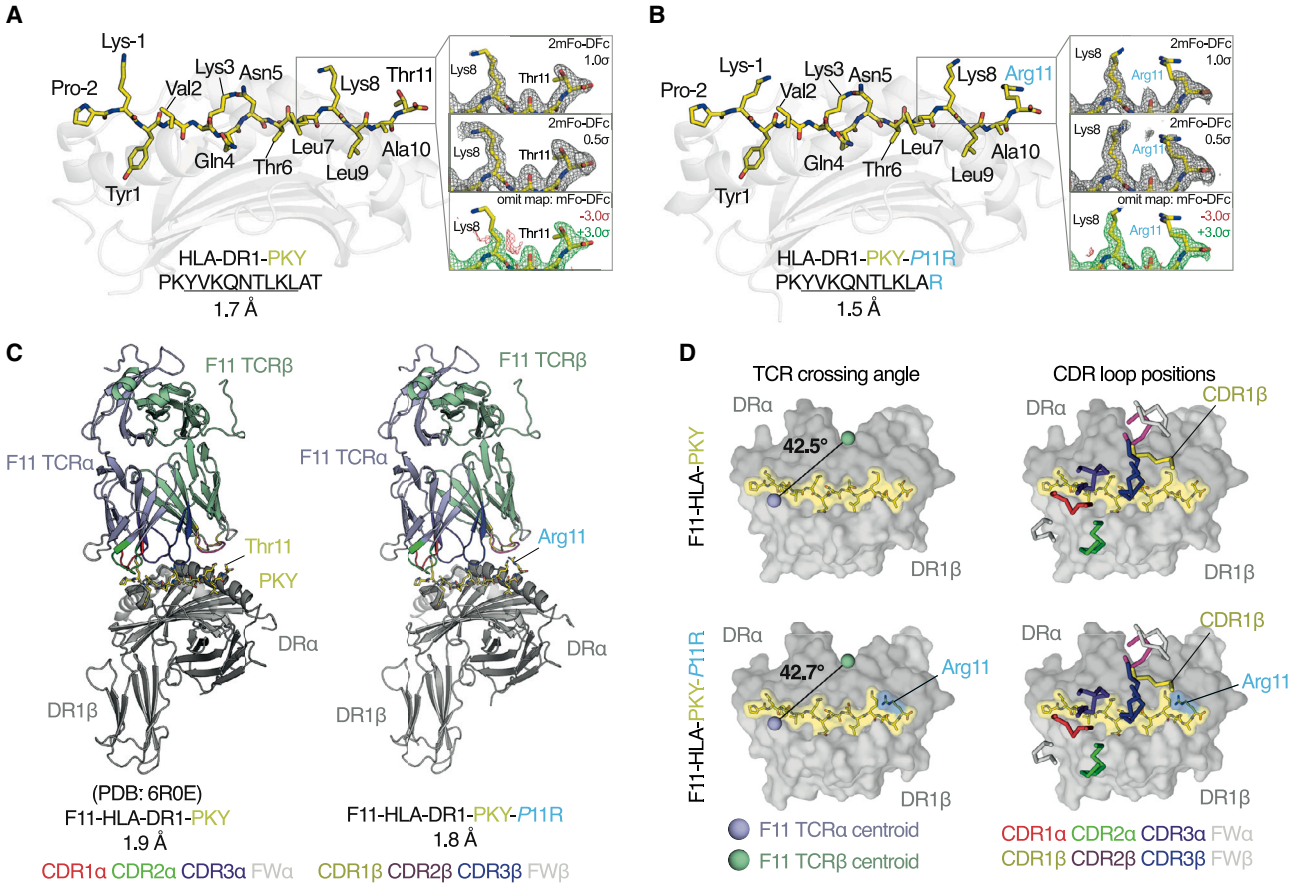

(legend on next page)

and hence the PFR, of a series of HLA-DR1-restricted immunodominant epitopes from several IAV-expressed proteins,[35] we used reverse genetics to generate modified whole A/X31 (H3N2) viruses incorporating C-terminal PFR changes at *P*11 (*P*11R). Some of these mutations markedly reduced viral replicative fitness, particularly if the internal proteins were targeted, in keeping with the more conserved nature of these proteins across viral subtypes. However, a T*P*11R substitution within an epitope from the external structural protein HA ($HA_{320-335}$) created a viable virus (labeled X31-HA-PKY) to test in transgenic HLA-DR1 mice.

The $HA_{320-335}$ epitope is an attractive candidate due to its characterization as an immunodominant epitope[50] and a promiscuous ligand, binding to multiple HLA-DR subtypes.[51] Furthermore, we have also demonstrated in human samples that synthetic peptide epitopes with the T*P*11R substitution alter T cell activation, seemingly by increasing TCR affinity for the pHLA-II complex.[34] Mice intranasally infected with 200 PFUs of X31-HA-PKY demonstrated significantly less weight loss and almost no clinical symptoms compared to those with A/X31 challenge. Indeed, 20% of A/X31-infected mice died or had to be sacrificed due to severe weight loss between days 8 and 10 post-infection (Figure 2). Measurement of cognate T cells in splenocytes and lung tissue by IFN-γ ELISpot or tetramer staining revealed an increase in $CD4^+$ T cell responses compared to A/X31-infected mice. Furthermore, X31-HA-PKY-infected mice had superior $CD8^+$ T cell responses, particularly directed against the immunodominant H2-D^b-restricted $NP_{366-374}$ epitope, measured at both day 8 (Figure S5) and then the later memory phase at day 62 (Figure 4A) post-infection.

The implication of this is that an increased IFN-γ^+ $CD4^+$ T cell response to a single epitope from one protein (HA) is sufficient to drive an increase in T cell responses to other viral proteins, including a $CD8^+$ T cell response focused on the internal NP ($NP_{366-374}$). The importance of this is further emphasized after a heterosubtypic challenge with the more virulent PR8 virus (H1N1) 2 months later, whereby X31-HA-PKY-primed mice have a better clinical outcome (Figure 3), likely helped by the increased population of long-lived lung tissue-resident H2-D^b-$NP_{366-374}$ $CD8^+$ T cells after primary infection.

This superior protective immunity against clinical symptoms raises a series of interesting points. Antigen remains a critical component of the T cell response after an initial infection leading to the APC-T cell interaction, but persistence of high levels of antigen would be detrimental.[52] However, this is not the case with *P*11R epitope modifications. Such amino acid changes do not increase peptide binding affinity to HLA-II antigens[45]: the alteration of the PFR can, however, select out different clonotypic expansions via altered TCR:pHLA affinities, numerically increasing the T cell expansion and concomitant IFN-γ production.[34] Not only are these $CD4^+$ T cells directly involved as anti-viral effectors, but the increased T cell-derived IFN-γ is known to generate a higher frequency of protective IAV-specific lung-resident $CD69^+$ $CD103^+$ $CD8^+$ memory T cells.[53] In addition, as effector $CD4^+$ T cells employ multiple mechanisms to control IAV, and because memory $CD4^+$ T cells seem to differ little from the rested effectors from which they are derived,[54] it seems the increased expansion of anti-viral $CD4^+$ T cells after primary infection will also impact the memory $CD4^+$ T cells, contributing to the better protection from further infections. The implications of these results are important, as cross-reactive $CD4^+$ and $CD8^+$ T cell immunity alters the clinical course of influenza in humans,[14,55] and in particular, tissue residency of anti-viral T cells in the lungs offers superior protection.[56]

To gain insight into how *P*11R modification may influence the presentation and recognition of the PKY epitope in HLA-DR1 humanized mice along with our previous work in humans,[34,39] we conducted structural analyses of WT and 11R-modified peptides bound by HLA-DR1. The binary structures of HLA-DR1-PKY versus PKY-*P*11R modification revealed very similar complexes. However, ternary structures with the TCR bound to pHLA-II demonstrated that subtle changes occur with the *P*11R peptide, including altered contacts between peptide residues at *P*8 and *P*11 with the TCRβ CDR1 loop. Thus, in the context of our previous TCR-clonotyping data describing PKY-specific TCRs in HLA-DR1+ donors,[35] our structural data indicate that a germline-encoded negative acidic amino acid motif within PKY-specific TCRs may be particularly predisposed to the influence of positive basic charges within the C-terminal PFR (murine TRBV

Figure 5. The ternary structure reveals mechanisms of increased TCR affinity for $HA_{320-335}$-*P*11R via interactions with the germline-encoded VβCDR1

(A) Structural overview of HLA-DR1 presenting WT $HA_{320-335}$ peptide. The HLA-II groove is shown as cartoon representation (gray), and peptide is shown as sticks (C atoms = yellow, N = blue, O = red). Peptide residues are labeled according to the peptide register, i.e., Tyr1 in *P*1. Inset boxes show a focused view of the C-PFR with inset labeled electron density maps as a mesh representation: 2mFo-DFc maps contoured at 1.0 (top) and 0.5 σ (middle) and mFo-DFc omit map, which was calculated in the absence of peptide atoms (bottom; -3.0 σ = red, +3.0 σ = green).

(B) Overview of HLA-DR1 presenting the modified *P*11R peptide. Represented as described in (A).

(C) Structural overview of F11-HLA-DR1-$HA_{320-335}$ (PDB: 6R0E) and F11-HLA-DR1-$HA_{320-335}$-*P*11R (this study). HLA-DR1 and F11-TCR are shown as cartoons (colored as inset) and $HA_{320-335}$ WT/*P*11R shown as sticks.

(D) Overview of F11 binding to HLA-DR1-$HA_{320-335}$ WT/*P*11R. The crossing angle (left) of TCRα and TCRβ centroids is shown (spheres) across the pHLA surface, and the angle in relation to the HLA groove is indicated in the inset. The overall CDR loop positions (Cα atom trace) is shown (right). Each CDR loop is colored as indicated by the inset.

(E) An expanded view of F11-CDR1β above the C-PFR of HLA-DR1-$HA_{320-335}$-*P*11R with indication of side chain charge (red = acidic, blue = basic) and residue position using IMGT numbering scheme.

(F) Alteration to contact network at F11-CDR1β interface with PKY under *P*11R modification. CDR1β and peptide atoms are shown as sticks. Salt bridge interactions (red; 4.0 A° cutoff), hydrogen bonds (blue; 3.5 A° cutoff), and van der Waals (black; <4.0 A° cutoff) are shown. Water molecules are shown as red spheres. Repulsive forces are indicated by inverted brackets (blue).

(G) F11-HLA-DR1-$HA_{320-335}$ electron density maps of F11-CDR1β interactions described in (F). 2mFo-DFc and mFo-DFc omit maps are as described in (B). All peptides, F11-CDR1β, and displayed water atoms were removed during omit map calculation.

(H) F11-HLA-DR1-$HA_{320-335}$-11R electron density maps as described in (G).

genes also contain acidic amino acid-containing CDR1β loops, e.g., TRBV4, TRBV8, TRBV13-3, TRBV14, TRBV17, TRBV19, and TRBV29).[57] Future work is planned to examine TCR repertoires in these mice.

In summary, these results show that priming mice with a live virus containing just a single targeted mutation in an MHC class II epitope enhances both the control of primary infection, and, importantly, long-term immunity, by impacting the memory population measured from lung-derived T cells. Experiments giving mice intranasal (but not intraperitoneal or subcutaneous) live attenuated IAV as a vaccine have demonstrated the importance of T_{RM} cells for immunity.[58] This approach could represent a strategy for improving influenza vaccine design.

Limitations of the study

This study employs transgenic HLA-DR1 mice to test manipulation of known HLA-DR1 influenza-derived epitopes by infecting mice with a murine-adapted seasonal H3N2 influenza virus (A/X31) genetically engineered to contain these known enhancing substitutions. The mice show markedly improved clinical scores after primary infection and superior long-term immunity with (heterosubtypic PR8 virus H1N1) re-challenge compared to A/X31-WT infected mice. Enhanced protection appeared to be mediated by lung-derived memory $CD4^+$and $CD8^+$ T cells. Although we previously fine-mapped other immunodominant HLA-DR1-restricted epitopes from IAV, this study did focus on the universal epitope $HA_{320-335}$, in part due to technical reasons, as targeting other epitopes impacted virus replication fitness. A mechanistic insight was gained from comparing ternary structures of the cognate TCR bound to pHLA-DR1 presenting either the WT or modified epitope, although this used a human rather than mouse cloned recombinant TCR.

STAR★METHODS

Detailed methods are provided in the online version of this paper and include the following:

SUPPLEMENTAL INFORMATION

Supplemental information can be found online at https://doi.org/10.1016/j.celrep.2024.114259.

ACKNOWLEDGMENTS

This work was supported by a Wellcome Trust Collaborative Award in Science (209213/Z/17/Z) led by A. Godkin. B.J.M. is supported by a Health and Care Research Wales - Health Research Fellowship (HF-21-1886). The authors would like to thank Diamond Light Source for beamtime (proposals mx10462 and mx14843) and the staff of beamline i03 for assistance with data collection. We thank the NIH Tetramer Core Facility for providing H2-D^b tetramers.

AUTHOR CONTRIBUTIONS

Conception or design of the work, A. Godkin, A. Gallimore, D.K.C., I.R.H., I.M.J., R.J.S., W.S.B., and S.H.-C.; acquisition, analysis, or interpretation of data, A. Godkin, A. Gallimore, S.H.-C., J.K.G., B.J.M., D.M.A., L.B., A.G.-W., S.J.H., S.N.L., G.H.M., K.S., D.O.S., J.S., K.S., A.W., and P.J.R.; drafting or substantively revising the manuscript, S.H.-C., J.K.G., A. Gallimore, and A. Godkin.

DECLARATION OF INTERESTS

The authors declare no competing interests.

Received: September 10, 2023
Revised: February 22, 2024
Accepted: May 6, 2024

REFERENCES

1. WHO (2018). Influenza (Seasonal). (seasonal). https://www.who.int/news-room/fact-sheets/detail/influenza-.
2. Altenburg, A.F., Rimmelzwaan, G.F., and de Vries, R.D. (2015). Virus-specific T cells as correlate of (cross-)protective immunity against influenza. Vaccine *33*, 500–506. https://doi.org/10.1016/j.vaccine.2014.11.054.
3. Zens, K.D., and Farber, D.L. (2015). Memory CD4 T cells in influenza. Curr. Top. Microbiol. Immunol. *386*, 399–421. https://doi.org/10.1007/82_2014_401.
4. Sant, A.J., DiPiazza, A.T., Nayak, J.L., Rattan, A., and Richards, K.A. (2018). CD4 T cells in protection from influenza virus: Viral antigen specificity and functional potential. Immunol. Rev. *284*, 91–105. https://doi.org/10.1111/imr.12662.
5. Sant, A.J., Richards, K.A., and Nayak, J. (2018). Distinct and complementary roles of CD4 T cells in protective immunity to influenza virus. Curr. Opin. Immunol. *53*, 13–21. https://doi.org/10.1016/j.coi.2018.03.019.
6. Jansen, J.M., Gerlach, T., Elbahesh, H., Rimmelzwaan, G.F., and Saletti, G. (2019). Influenza virus-specific CD4+ and CD8+ T cell-mediated immunity induced by infection and vaccination. J. Clin. Virol. *119*, 44–52. https://doi.org/10.1016/j.jcv.2019.08.009.
7. Sant, A.J., and McMichael, A. (2012). Revealing the role of CD4(+) T cells in viral immunity. J. Exp. Med. *209*, 1391–1395. https://doi.org/10.1084/jem.20121517.
8. Eichelberger, M., Allan, W., Zijlstra, M., Jaenisch, R., and Doherty, P.C. (1991). Clearance of influenza virus respiratory infection in mice lacking

class I major histocompatibility complex-restricted CD8+ T cells. J. Exp. Med. *174*, 875–880. https://doi.org/10.1084/jem.174.4.875.

9. Swain, S.L., McKinstry, K.K., and Strutt, T.M. (2012). Expanding roles for CD4(+) T cells in immunity to viruses. Nat. Rev. Immunol. *12*, 136–148. https://doi.org/10.1038/nri3152.
10. Strutt, T.M., McKinstry, K.K., Dibble, J.P., Winchell, C., Kuang, Y., Curtis, J.D., Huston, G., Dutton, R.W., and Swain, S.L. (2010). Memory CD4+ T cells induce innate responses independently of pathogen. Nat. Med. *16*, 558–564. https://doi.org/10.1038/nm.2142.
11. Boyden, A.W., Legge, K.L., and Waldschmidt, T.J. (2012). Pulmonary infection with influenza A virus induces site-specific germinal center and T follicular helper cell responses. PLoS One *7*, e40733. https://doi.org/10.1371/journal.pone.0040733.
12. Brown, D.M., Lee, S., Garcia-Hernandez, M.d.l.L., and Swain, S.L. (2012). Multifunctional CD4 cells expressing gamma interferon and perforin mediate protection against lethal influenza virus infection. J. Virol. *86*, 6792–6803. https://doi.org/10.1128/JVI.07172-11.
13. Brown, D.M., Dilzer, A.M., Meents, D.L., and Swain, S.L. (2006). CD4 T cell-mediated protection from lethal influenza: perforin and antibody-mediated mechanisms give a one-two punch. J. Immunol. *177*, 2888–2898. https://doi.org/10.4049/jimmunol.177.5.2888.
14. Wilkinson, T.M., Li, C.K.F., Chui, C.S.C., Huang, A.K.Y., Perkins, M., Liebner, J.C., Lambkin-Williams, R., Gilbert, A., Oxford, J., Nicholas, B., et al. (2012). Preexisting influenza-specific CD4+ T cells correlate with disease protection against influenza challenge in humans. Nat. Med. *18*, 274–280. https://doi.org/10.1038/nm.2612.
15. Brown, D.M., Lampe, A.T., and Workman, A.M. (2016). The Differentiation and Protective Function of Cytolytic CD4 T Cells in Influenza Infection. Front. Immunol. *7*, 93. https://doi.org/10.3389/fimmu.2016.00093.
16. Juno, J.A., van Bockel, D., Kent, S.J., Kelleher, A.D., Zaunders, J.J., and Munier, C.M.L. (2017). Cytotoxic CD4 T Cells-Friend or Foe during Viral Infection? Front. Immunol. *8*, 19. https://doi.org/10.3389/fimmu.2017.00019.
17. McKinstry, K.K., Strutt, T.M., Kuang, Y., Brown, D.M., Sell, S., Dutton, R.W., and Swain, S.L. (2012). Memory CD4+ T cells protect against influenza through multiple synergizing mechanisms. J. Clin. Invest. *122*, 2847–2856. https://doi.org/10.1172/JCI63689.
18. Epstein, S.L., and Price, G.E. (2010). Cross-protective immunity to influenza A viruses. Expert Rev. Vaccines *9*, 1325–1341. https://doi.org/10.1586/erv.10.123.
19. Couch, R.B. (2003). Challenge studies. Dev. Biol. *115*, 119–121.
20. Kurtz, J.R., Petersen, H.E., Frederick, D.R., Morici, L.A., and McLachlan, J.B. (2014). Vaccination with a single CD4 T cell peptide epitope from a Salmonella type III-secreted effector protein provides protection against lethal infection. Infect. Immun. *82*, 2424–2433. https://doi.org/10.1128/IAI.00052-14.
21. Smiley, K.L., McNeal, M.M., Basu, M., Choi, A.H.C., Clements, J.D., and Ward, R.L. (2007). Association of gamma interferon and interleukin-17 production in intestinal CD4+ T cells with protection against rotavirus shedding in mice intranasally immunized with VP6 and the adjuvant LT(R192G). J. Virol. *81*, 3740–3748. https://doi.org/10.1128/JVI.01877-06.
22. Wada, Y., Nithichanon, A., Nobusawa, E., Moise, L., Martin, W.D., Yamamoto, N., Terahara, K., Hagiwara, H., Odagiri, T., Tashiro, M., et al. (2017). A humanized mouse model identifies key amino acids for low immunogenicity of H7N9 vaccines. Sci. Rep. *7*, 1283. https://doi.org/10.1038/s41598-017-01372-5.
23. Pop-Vicas, A., and Gravenstein, S. (2011). Influenza in the elderly: a mini-review. Gerontology *57*, 397–404. https://doi.org/10.1159/000319033.
24. Buchy, P., and Badur, S. (2020). Who and when to vaccinate against influenza. Int. J. Infect. Dis. *93*, 375–387. https://doi.org/10.1016/j.ijid.2020.02.040.
25. Sheth, A.N., Patel, P., and Peters, P.J. (2011). Influenza and HIV: lessons from the 2009 H1N1 influenza pandemic. Curr. HIV AIDS Rep. *8*, 181–191. https://doi.org/10.1007/s11904-011-0086-4.
26. Caldera, F., Mercer, M., Samson, S.I., Pitt, J.M., and Hayney, M.S. (2021). Influenza vaccination in immunocompromised populations: Strategies to improve immunogenicity. Vaccine *39*, A15–A23. https://doi.org/10.1016/j.vaccine.2020.11.037.
27. Jang, Y.H., and Seong, B.L. (2019). The Quest for a Truly Universal Influenza Vaccine. Front. Cell. Infect. Microbiol. *9*, 344. https://doi.org/10.3389/fcimb.2019.00344.
28. Lamb, J.R., Eckels, D.D., Lake, P., Johnson, A.H., Hartzman, R.J., and Woody, J.N. (1982). Antigen-specific human T lymphocyte clones: induction, antigen specificity, and MHC restriction of influenza virus-immune clones. J. Immunol. *128*, 233–238.
29. Krieger, J.I., Karr, R.W., Grey, H.M., Yu, W.Y., O'Sullivan, D., Batovsky, L., Zheng, Z.L., Colón, S.M., Gaeta, F.C., Sidney, J., et al. (1991). Single amino acid changes in DR and antigen define residues critical for peptide-MHC binding and T cell recognition. J. Immunol. *146*, 2331–2340.
30. Roche, P.A., and Cresswell, P. (1990). High-affinity binding of an influenza hemagglutinin-derived peptide to purified HLA-DR. J. Immunol. *144*, 1849–1856.
31. Carson, R.T., Vignali, K.M., Woodland, D.L., and Vignali, D.A. (1997). T cell receptor recognition of MHC class II-bound peptide flanking residues enhances immunogenicity and results in altered TCR V region usage. Immunity *7*, 387–399. https://doi.org/10.1016/s1074-7613(00)80360-x.
32. Holland, C.J., Cole, D.K., and Godkin, A. (2013). Re-Directing CD4(+) T Cell Responses with the Flanking Residues of MHC Class II-Bound Peptides: The Core is Not Enough. Front. Immunol. *4*, 172. https://doi.org/10.3389/fimmu.2013.00172.
33. Godkin, A.J., Davenport, M.P., Willis, A., Jewell, D.P., and Hill, A.V. (1998). Use of complete eluted peptide sequence data from HLA-DR and -DQ molecules to predict T cell epitopes, and the influence of the nonbinding terminal regions of ligands in epitope selection. J. Immunol. *161*, 850–858.
34. Cole, D.K., Gallagher, K., Lemercier, B., Holland, C.J., Junaid, S., Hindley, J.P., Wynn, K.K., Gostick, E., Sewell, A.K., Gallimore, A.M., et al. (2012). Modification of the carboxy-terminal flanking region of a universal influenza epitope alters CD4(+) T-cell repertoire selection. Nat. Commun. *3*, 665. https://doi.org/10.1038/ncomms1665.
35. Greenshields-Watson, A., Attaf, M., MacLachlan, B.J., Whalley, T., Rius, C., Wall, A., Lloyd, A., Hughes, H., Strange, K.E., Mason, G.H., et al. (2020). CD4(+) T Cells Recognize Conserved Influenza A Epitopes through Shared Patterns of V-Gene Usage and Complementary Biochemical Features. Cell Rep. *32*, 107885. https://doi.org/10.1016/j.celrep.2020.107885.
36. Altmann, D.M., Douek, D.C., Frater, A.J., Hetherington, C.M., Inoko, H., and Elliott, J.I. (1995). The T cell response of HLA-DR transgenic mice to human myelin basic protein and other antigens in the presence and absence of human CD4. J. Exp. Med. *181*, 867–875. https://doi.org/10.1084/jem.181.3.867.
37. Chen, W., Pang, K., Masterman, K.A., Kennedy, G., Basta, S., Dimopoulos, N., Hornung, F., Smyth, M., Bennink, J.R., and Yewdell, J.W. (2004). Reversal in the immunodominance hierarchy in secondary CD8+ T cell responses to influenza A virus: roles for cross-presentation and lysis-independent immunodomination. J. Immunol. *173*, 5021–5027. https://doi.org/10.4049/jimmunol.173.8.5021.
38. Belz, G.T., Xie, W., Altman, J.D., and Doherty, P.C. (2000). A previously unrecognized H-2D(b)-restricted peptide prominent in the primary influenza A virus-specific CD8(+) T-cell response is much less apparent following

secondary challenge. J. Virol. *74*, 3486–3493. https://doi.org/10.1128/Jvi.74.8.3486-3493.2000.

39. Holland, C.J., Dolton, G., Scurr, M., Ladell, K., Schauenburg, A.J., Miners, K., Madura, F., Sewell, A.K., Price, D.A., Cole, D.K., and Godkin, A.J. (2015). Enhanced Detection of Antigen-Specific CD4+ T Cells Using Altered Peptide Flanking Residue Peptide-MHC Class II Multimers. J. Immunol. *195*, 5827–5836. https://doi.org/10.4049/jimmunol.1402787.
40. Lamb, J.R., Eckels, D.D., Lake, P., Woody, J.N., and Green, N. (1982). Human T-cell clones recognize chemically synthesized peptides of influenza haemagglutinin. Nature *300*, 66–69. https://doi.org/10.1038/300066a0.
41. Lamb, J.R., and Green, N. (1983). Analysis of the antigen specificity of influenza haemagglutinin-immune human T lymphocyte clones: identification of an immunodominant region for T cells. Immunology *50*, 659–666.
42. Eckels, D.D., Sell, T.W., Bronson, S.R., Johnson, A.H., Hartzman, R.J., and Lamb, J.R. (1984). Human helper T-cell clones that recognize different influenza hemagglutinin determinants are restricted by different HLA-D region epitopes. Immunogenetics *19*, 409–423. https://doi.org/10.1007/BF00364644.
43. Rajnavolgyi, E., Horvath, A., Gogolak, P., Toth, G.K., Fazekas, G., Fridkin, M., and Pecht, I. (1997). Characterizing immunodominant and protective influenza hemagglutinin epitopes by functional activity and relative binding to major histocompatibility complex class II sites. Eur. J. Immunol. *27*, 3105–3114. https://doi.org/10.1002/eji.1830271205.
44. Stern, L.J., Brown, J.H., Jardetzky, T.S., Gorga, J.C., Urban, R.G., Strominger, J.L., and Wiley, D.C. (1994). Crystal structure of the human class II MHC protein HLA-DR1 complexed with an influenza virus peptide. Nature *368*, 215–221. https://doi.org/10.1038/368215a0.
45. MacLachlan, B.J., Dolton, G., Papakyriakou, A., Greenshields-Watson, A., Mason, G.H., Schauenburg, A., Besneux, M., Szomolay, B., Elliott, T., Sewell, A.K., et al. (2019). Human leukocyte antigen (HLA) class II peptide flanking residues tune the immunogenicity of a human tumor-derived epitope. J. Biol. Chem. *294*, 20246–20258. https://doi.org/10.1074/jbc.RA119.009437.
46. Rudolph, M.G., Stanfield, R.L., and Wilson, I.A. (2006). How TCRs bind MHCs, peptides, and coreceptors. Annu. Rev. Immunol. *24*, 419–466. https://doi.org/10.1146/annurev.immunol.23.021704.115658.
47. Arnold, P.Y., La Gruta, N.L., Miller, T., Vignali, K.M., Adams, P.S., Woodland, D.L., and Vignali, D.A.A. (2002). The majority of immunogenic epitopes generate CD4+ T cells that are dependent on MHC class II-bound peptide-flanking residues. J. Immunol. *169*, 739–749. https://doi.org/10.4049/jimmunol.169.2.739.
48. Moudgil, K.D., Wang, J., Yeung, V.P., and Sercarz, E.E. (1998). Heterogeneity of the T cell response to immunodominant determinants within hen eggwhite lysozyme of individual syngeneic hybrid F1 mice: implications for autoimmunity and infection. J. Immunol. *161*, 6046–6053.
49. Godkin, A.J., Smith, K.J., Willis, A., Tejada-Simon, M.V., Zhang, J., Elliott, T., and Hill, A.V. (2001). Naturally processed HLA class II peptides reveal highly conserved immunogenic flanking region sequence preferences that reflect antigen processing rather than peptide-MHC interactions. J. Immunol. *166*, 6720–6727. https://doi.org/10.4049/jimmunol.166.11.6720.
50. O'Sullivan, D., Arrhenius, T., Sidney, J., Del Guercio, M.F., Albertson, M., Wall, M., Oseroff, C., Southwood, S., Colón, S.M., Gaeta, F.C., et al. (1991). On the interaction of promiscuous antigenic peptides with different DR alleles. Identification of common structural motifs. J. Immunol. *147*, 2663–2669.
51. Fu, X.T., Bono, C.P., Woulfe, S.L., Swearingen, C., Summers, N.L., Sinigaglia, F., Sette, A., Schwartz, B.D., and Karr, R.W. (1995). Pocket 4 of the HLA-DR(alpha,beta 1*0401) molecule is a major determinant of T cells recognition of peptide. J. Exp. Med. *181*, 915–926. https://doi.org/10.1084/jem.181.3.915.
52. Bassil, R., Zhu, B., Lahoud, Y., Riella, L.V., Yagita, H., Elyaman, W., and Khoury, S.J. (2011). Notch ligand delta-like 4 blockade alleviates experimental autoimmune encephalomyelitis by promoting regulatory T cell development. J. Immunol. *187*, 2322–2328. https://doi.org/10.4049/jimmunol.1100725.
53. Laidlaw, B.J., Zhang, N., Marshall, H.D., Staron, M.M., Guan, T., Hu, Y., Cauley, L.S., Craft, J., and Kaech, S.M. (2014). CD4+ T cell help guides formation of CD103+ lung-resident memory CD8+ T cells during influenza viral infection. Immunity *41*, 633–645. https://doi.org/10.1016/j.immuni.2014.09.007.
54. Woodland, D.L., Hogan, R.J., and Zhong, W. (2001). Cellular immunity and memory to respiratory virus infections. Immunol. Res. *24*, 53–67. https://doi.org/10.1385/IR:24:1:53.
55. Sridhar, S., Begom, S., Bermingham, A., Hoschler, K., Adamson, W., Carman, W., Bean, T., Barclay, W., Deeks, J.J., and Lalvani, A. (2013). Cellular immune correlates of protection against symptomatic pandemic influenza. Nat. Med. *19*, 1305–1312. https://doi.org/10.1038/nm.3350.
56. Pizzolla, A., Nguyen, T.H., Sant, S., Jaffar, J., Loudovaris, T., Mannering, S.I., Thomas, P.G., Westall, G.P., Kedzierska, K., and Wakim, L.M. (2018). Influenza-specific lung-resident memory T cells are proliferative and polyfunctional and maintain diverse TCR profiles. J. Clin. Invest. *128*, 721–733. https://doi.org/10.1172/JCI96957.
57. Lefranc, M.P., Giudicelli, V., Duroux, P., Jabado-Michaloud, J., Folch, G., Aouinti, S., Carillon, E., Duvergey, H., Houles, A., Paysan-Lafosse, T., et al. (2015). IMGT(R), the international ImMunoGeneTics information system(R) 25 years on. Nucleic Acids Res. *43*, D413–D422. https://doi.org/10.1093/nar/gku1056.
58. Zens, K.D., Chen, J.K., and Farber, D.L. (2016). Vaccine-generated lung tissue-resident memory T cells provide heterosubtypic protection to influenza infection. JCI Insight *1*, e85832. https://doi.org/10.1172/jci.insight.85832.
59. Bulek, A.M., Madura, F., Fuller, A., Holland, C.J., Schauenburg, A.J.A., Sewell, A.K., Rizkallah, P.J., and Cole, D.K. (2012). TCR/pMHC Optimized Protein crystallization Screen. J. Immunol. Methods *382*, 203–210. https://doi.org/10.1016/j.jim.2012.06.007.
60. Hoffmann, E., Neumann, G., Kawaoka, Y., Hobom, G., and Webster, R.G. (2000). A DNA transfection system for generation of influenza A virus from eight plasmids. Proc. Natl. Acad. Sci. USA *97*, 6108–6113. https://doi.org/10.1073/pnas.100133697.
61. Holland, C.J., MacLachlan, B.J., Bianchi, V., Hesketh, S.J., Morgan, R., Vickery, O., Bulek, A.M., Fuller, A., Godkin, A., Sewell, A.K., et al. (2018). In Silico and Structural Analyses Demonstrate That Intrinsic Protein Motions Guide T Cell Receptor Complementarity Determining Region Loop Flexibility. Front. Immunol. *9*, 674. https://doi.org/10.3389/fimmu.2018.00674.
62. Boulter, J.M., Glick, M., Todorov, P.T., Baston, E., Sami, M., Rizkallah, P., and Jakobsen, B.K. (2003). Stable, soluble T-cell receptor molecules for crystallization and therapeutics. Protein Eng. *16*, 707–711. https://doi.org/10.1093/protein/gzg087.
63. Winter, G., Lobley, C.M.C., and Prince, S.M. (2013). Decision making in xia2. Acta Crystallogr. D Biol. Crystallogr. *69*, 1260–1273. https://doi.org/10.1107/S0907444913015308.
64. Winter, G., Waterman, D.G., Parkhurst, J.M., Brewster, A.S., Gildea, R.J., Gerstel, M., Fuentes-Montero, L., Vollmar, M., Michels-Clark, T., Young, I.D., et al. (2018). DIALS: implementation and evaluation of a new integration package. Acta Crystallogr. D Struct. Biol. *74*, 85–97. https://doi.org/10.1107/S2059798317017235.
65. Kabsch, W. (2010). Xds. Acta Crystallogr. D Biol. Crystallogr. *66*, 125–132. https://doi.org/10.1107/S0907444909047337.
66. Evans, P. (2006). Scaling and assessment of data quality. Acta Crystallogr. D Biol. Crystallogr. *62*, 72–82. https://doi.org/10.1107/S0907444905036693.

67. Evans, P.R., and Murshudov, G.N. (2013). How good are my data and what is the resolution? Acta Crystallogr. D Biol. Crystallogr. *69*, 1204–1214. https://doi.org/10.1107/S0907444913000061.

68. McCoy, A.J. (2007). Solving structures of protein complexes by molecular replacement with Phaser. Acta Crystallogr. D Biol. Crystallogr. *63*, 32–41. https://doi.org/10.1107/S0907444906045975.

69. Liebschner, D., Afonine, P.V., Baker, M.L., Bunkóczi, G., Chen, V.B., Croll, T.I., Hintze, B., Hung, L.W., Jain, S., McCoy, A.J., et al. (2019). Macromolecular structure determination using X-rays, neutrons and electrons: recent developments in Phenix. Acta Crystallogr. D Struct. Biol. *75*, 861–877. https://doi.org/10.1107/S2059798319011471.

70. Emsley, P., and Cowtan, K. (2004). Coot: model-building tools for molecular graphics. Acta Crystallogr. D Biol. Crystallogr. *60*, 2126–2132. https://doi.org/10.1107/S0907444904019158.

71. Williams, C.J., Headd, J.J., Moriarty, N.W., Prisant, M.G., Videau, L.L., Deis, L.N., Verma, V., Keedy, D.A., Hintze, B.J., Chen, V.B., et al. (2018). MolProbity: More and better reference data for improved all-atom structure validation. Protein Sci. *27*, 293–315. https://doi.org/10.1002/pro.3330.

STAR★METHODS

KEY RESOURCES TABLE

REAGENT or RESOURCE	SOURCE	IDENTIFIER
Antibodies		
Brilliant Violet 785 Anti-Mouse CD3 [Clone: 17A2]	Biolegend	Cat#100232 RRID: AB_2562554
Brilliant Violet 605 Anti-Mouse CD19 [Clone: 6D5]	Biolegend	Cat#115540 RRID: AB_2563067
APC Anti-Mouse CD4 [Clone: GK1.5]	Biolegend	Cat#100412 RRID: AB_312697
Brilliant Violet 421 Anti-Mouse CD8a [Clone: 53–6.7]	Biolegend	Cat#100738 RRID: AB_11204079
APC/Fire 750 Anti-Mouse CD69 [Clone: H1.2F3]	Biolegend	Cat#104549 RRID: AB_2800560
BD OptiBuild BV650 Hamster Anti-Mouse CD103 [Clone: 2E7]	BD Biosciences	Cat#748256 RRID: AB_2872685
TruStain FcX Anti-Mouse CD16/32 [Clone: 93]	Biolegend	Cat#101320 RRID: AB_1574975
Ultra-LEAF™ Purified anti-human HLA-DR Antibody	Biolegend	Cat#307667 RRID:AB_2800798
Bacterial and virus strains		
Escherichia coli BL21(DE3) Chemically Competent cells	ThermoFisher Scientific	Cat#C600003
NEB® 5-alpha Competent E. coli (High Efficiency)	New England Biolabs	Cat# C2987I
X31 Influenza A Virus	Laboratory of Wendy Barclay	A/Aichi/2/68 [H3N2]
Recombinant X31-HA-PKY Influenza A Virus	Laboratory of Wendy Barclay	A/Aichi/2/68 [H3N2]
PR8 Influenza A Virus	Laboratory of Wendy Barclay	A/Puerto Rico/8/34 [H1N1]
Chemicals, peptides, and recombinant proteins		
Synthetic peptide PKY (structural studies) PKYVKQNTLKLAT	Peptide Protein Research	Custom synthesis
Synthetic peptide PKY-11R (structural studies) PKYVKQNTLKLAR	Peptide Protein Research	Custom synthesis
Synthetic peptide SGP [M1 17–31] (ELISpot assays) - SGPLKAEIAQRLEDV	GL Biochem (Shanghai) Ltd.	Custom Synthesis Cat#296326
Synthetic peptide GLI [M1 129–143] (ELISpot assays) - GLIYNRMGAVTTEVA	GL Biochem (Shanghai) Ltd.	Custom Synthesis Cat#715911
Synthetic peptide QAR [M1 210–224] (ELISpot assays) - RQMVQAMRTIGTHPS	GL Biochem (Shanghai) Ltd.	Custom Synthesis Cat#715917
Synthetic peptide NAE [NP 254–268] (ELISpot assays) - EDLIFLARSALILRG	GL Biochem (Shanghai) Ltd.	Custom Synthesis Cat#662255
Synthetic peptide DPF [NP 301–315] (ELISpot assays/Monomer Production) - IDPFRLLQNSQVFSL	GL Biochem (Shanghai) Ltd.	Custom Synthesis Cat#715921
Synthetic peptide NPR [PB1 315–329] (ELISpot assays) - PRMFLAMITYMTRNQ	GL Biochem (Shanghai) Ltd.	Custom Synthesis Cat#716106
Synthetic peptide GMF [PB1 409–423] (ELISpot assays) - MGMFNMLSTVLGVSI	GL Biochem (Shanghai) Ltd.	Custom Synthesis Cat#715919
Synthetic peptide CYP [HA 118–132] (ELISpot assays) - VPDYASLRSLVASSG	GL Biochem (Shanghai) Ltd.	Custom Synthesis Cat#237703

(*Continued on next page*)

Continued

REAGENT or RESOURCE	SOURCE	IDENTIFIER
Synthetic peptide PKY [HA 320–335] (ELISpot assays) - APKYVKQNTLKLATG	GL Biochem (Shanghai) Ltd.	Custom Synthesis Cat#716094
Synthetic peptide GLI V11R [M1 129–143] (ELISpot assays) - GLIYNRMGAVTTERA	Peptide Protein Research	Custom Synthesis
Synthetic peptide DPF S11R [NP 301–315] (ELISpot assays/Monomer Production) - IDPFRLLQNSQVFRL	GL Biochem (Shanghai) Ltd.	Custom Synthesis Cat#716094
Synthetic peptide NPR N11R [NP 315–329] (ELISpot assays) - PRMFLAMITYMTRRQ	GL Biochem (Shanghai) Ltd.	Custom Synthesis Cat#716107
Synthetic peptide CYP S11R [HA 118–132] (ELISpot assays) - VPDYASLRSLVASRG	GL Biochem (Shanghai) Ltd.	Custom Synthesis Cat#716101
Synthetic peptide PKY T11R [HA 320–335] (ELISpot assays) - APKYVKQNTLKLARG	GL Biochem (Shanghai) Ltd.	Custom Synthesis Cat#716095
Synthetic peptide NAE R11A [NP 254–268] (ELISpot assays) - EDLIFLARSALILAG	GL Biochem (Shanghai) Ltd.	Custom Synthesis Cat#716104
Synthetic peptide ETM [NP 366–374] (ELISpot assays) - ASNENMETM	Peptide Protein Research	Custom Synthesis
Synthetic peptide SSL [PA 224–233] (ELISpot assays) - SSLENFRAYV	Peptide Protein Research	Custom Synthesis
Synthetic peptide LSL [PB1-F2 62–70] (ELISpot assays) - LSLRNPILV	Peptide Protein Research	Custom Synthesis
Biotinylated HLA-DR1 Monomer – DPF [NP 301–315] - IDPFRLLQNSQVFSL	This Manuscript	N/A
Biotinylated HLA-DR1 Monomer – DPF S11R [NP 301–315] - IDPFRLLQNSQVFRL	This Manuscript	N/A
Biotinylated HLA-DR1 Monomer – PKY [HA 320–335] - APKYVKQNTLKLATG	This Manuscript	N/A
Biotinylated HLA-DR1 Monomer – PKY T11R [HA 320–335] - APKYVKQNTLKLARG	This Manuscript	N/A
Biotinylated H2-D^b Monomer – ETM [NP 366–374] - ASNENMETM	NIH Tetramer Core Facility (Atlanta, USA)	Premade Class I Reagent
Biotinylated H2-D^b Monomer – SSL [PA 224–233] - SSLENFRAYV	NIH Tetramer Core Facility (Atlanta, USA)	Premade Class I Reagent
Biotinylated H2-D^b Monomer – LSL [PB1-F2 62–70] - LSLRNPILV	NIH Tetramer Core Facility (Atlanta, USA)	Custom Class I Reagent
PE-Streptavidin	Biolegend	Cat#405204
Dasatinib (BMS 354825)	Axon Medchem	Cat#1392
Pierce™ Protein A IgG Plus Orientation Kit, 2 mL	Thermo Scientific	Cat#44893
RPMI 1640	Sigma-Aldrich	Cat#R0883
Dulbecco′s Modified Eagle′s Medium	Sigma-Aldrich	Cat#D5796
Trypsin-EDTA	Sigma-Aldrich	Cat#T3924
MEM (10X) Gibco	Thermo Fisher Scientific (Life Technologies)	Cat#21430020
Bovine Serum Albumin Fraction V (7.5%)	Thermo Fisher Scientific (Life Technologies)	Cat#15260037
L-Glutamine (200 mM)	Fisher Scientific	Cat#15410314
$NaHCO_3$ (7.5%)	Thermo Fisher Scientific (Life Technologies)	Cat#25080094
Penicillin-Streptomycin	Fisher Scientific	Cat#11548876
HEPES Buffer (1M)	Sigma-Aldrich	Cat#83264
DEAE-Dextran	Sigma-Aldrich	Cat#80881
Crystal Violet	Sigma-Aldrich	Cat#C6158
Collagenase	Sigma-Aldrich	Cat#C5138
Turkey Blood Cells (Alsevers)	Envigo RMS (Oxfordshire)	Cat#S.B-0047

(*Continued on next page*)

Continued

REAGENT or RESOURCE	SOURCE	IDENTIFIER
Critical commercial assays		
TOPS Crystallization Screen	Molecular Dimensions	Custom product. Bulek et al.[59]
PACT premier™ HT-96 Crystallization Screen	Molecular Dimensions	Cat#MD1-36
ELISpot Flex: Mouse IFN-gamma (ALP)	Mabtech	Cat#3321-2A
ELISpot Substrate: BCIP/NBT-plus for ALP	Mabtech	Cat#3650-10
BirA Biotin-Protein Ligase Bulk Reaction Kit	Avidty	Cat# BirA500
Receptor Destroying Enzyme Kit	Cosmos Biomedical	Cat#CB50/340122
LIVE/DEAD™ Fixable Aqua Kit	Fisher Scientific	Cat#15511863
X-tremeGENE™ 360 Transfection Reagent	Sigma-Aldrich	Cat# XTG360-RO
QuikChange Lightning Site-Directed Kit	Agilent	Cat#210518
Deposited data		
HLA-DR1-PKY	This manuscript	PDB: 8PJE
HLA-DR1-PKY-11R	This manuscript	PDB: 8PJF
F11-HLA-DR1-PKY-11R	This manuscript	PDB: 8PJG
F11-HLA-DR1-PKY	Greenshields-Watson et al.	PDB: 6R0E
Experimental models: Cell lines		
MDCK	ATCC	Cat#CCL-34 RRID: CVCL_0422
HEK293T	ATCC	Cat#CRL-3216 RRID: CVCL_0063
Experimental models: Organisms/strains		
HLA-DR1+ Mice. Strain: Tg(HLA-DRA*0101, HLA-DRB1*0101) - C57BL/6 background	Laboratory of Daniel Altman	RRID: MGI_5312109
C57BL/6J Mice	Charles River UK	RRID: IMSR_JAX:000664
Oligonucleotides		
X31-HA-PKY Site-Directed Mutagenesis Primer: CCCTGAAGTTGGCACGAGGGA TGCGGAATGTACC	Laboratory of Wendy Barclay	N/A
Recombinant DNA		
pGEM-T7	Promega	Cat# A3600
pGEM-T7-DRA1*0101	Cole, Godkin labs	Greenshields-Watson et al.[35]
pGEM-T7-DRB1*0101	Cole, Godkin labs	Greenshields-Watson et al.[35]
pGEM-T7-F11-TCRa	Cole, Godkin labs	Cole et al.[34]
pGEM-T7-F11-TCRa	Cole, Godkin labs	Cole et al.[34]
pHW2000 Viral Segment 1 (PB2) - A/PR/8/34 [H1N1]	Provided by Dr J. Zhou (Barclay lab)	Hoffmann et al.[60]
pHW2000 Viral Segment 2 (PB1) - A/PR/8/34 [H1N1]	Provided by Dr J. Zhou (Barclay lab)	Hoffmann et al.[60]
pHW2000 Viral Segment 3 (PA) - A/PR/8/34 [H1N1]	Provided by Dr J. Zhou (Barclay lab)	Hoffmann et al.[60]
pHW2000 Viral Segment 5 (NP) - A/PR/8/34 [H1N1]	Provided by Dr J. Zhou (Barclay lab)	Hoffmann et al.[60]
pHW2000 Viral Segment 7 (M) - A/PR/8/34 [H1N1]	Provided by Dr J. Zhou (Barclay lab)	Hoffmann et al.[60]
pHW2000 Viral Segment 8 (NS) - A/PR/8/34 [H1N1]	Provided by Dr J. Zhou (Barclay lab)	Hoffmann et al.[60]
pHW2000 Viral Segment 4 (HA) - A/Aichi/2/1968 [H3N2]	Provided by Dr J. Zhou (Barclay lab)	Hoffmann et al.[60]

(*Continued on next page*)

Continued

REAGENT or RESOURCE	SOURCE	IDENTIFIER
pHW2000 Viral Segment 6 (NA) - A/Aichi/2/1968 [H3N2]	Provided by Dr J. Zhou (Barclay lab)	Hoffmann et al.[60]
pHW2000 Viral Segment 4 (HA-PKY) - A/Aichi/2/1968 [H3N2]	This manuscript	N/A
Software and algorithms		
PyMOL (v2.5 open-source build)	Maintained by Schrodinger	RRID: SCR_000305
Phaser	Phenix Online	RRID: SCR_014219
Phenix v1.20	Phenix Online	RRID: SCR_014224
CCP4	Collaborative Computational Project No. 4	RRID: SCR_007255
Molprobity	Duke University	RRID: SCR_014226
Xia2 pipeline	Diamond Light Source (DLS)	RRID: SCR_015746
Dials	DLS, Lawrence Berkeley National Laboratory and STFC	https://dials.github.io/about.html
XDS program package	Max Planck Institute for Medical Research	RRID: SCR_015652
COOT v0.9.6	MRC Laboratory of Molecular Biology	RRID: SCR_014222
FlowJo	FlowJo LLC	RRID: SCR_008520
GraphPad Prism	GraphPad Software Inc.	RRID: SCR_002798
Other		
Multiscreen-IP Filter Plate (For ELISpot)	Sigma-Aldrich	Cat#MAIPS4510

RESOURCE AVAILABILITY

Lead contact

Further information and requests for resources and reagents should be directed to and will be fulfilled by the lead contact, Professor Andrew Godkin (godkinaj@cardiff.ac.uk).

Materials availability

Recombinant viruses, cell lines and protein expression plasmids are available from the lead contact on request. All other reagents are available to purchase from commercial suppliers.

Data and code availability

- Final model co-ordinates and structure factors were submitted to the Protein DataBank under accession codes: DR1-PKY = 8PJE, DR1-PKY-11R = 8PJF, F11-DR1-PKY-11R = 8PJG, All other raw data are available from Mendeley Data at the following link: https://data.mendeley.com/datasets/wm43n6h5n3/1https://data.mendeley.com/datasets/wm43n6h5n3/1 (https://doi.org/10.17632/wm43n6h5n3.1).
- This paper does not report any original code.
- Any additional information required to reanalyze the data reported in this paper is available from the lead contact upon request.

EXPERIMENTAL MODEL AND STUDY PARTICIPANT DETAILS

Mice

HLA-DR1 transgenic mice (HLA-DRA*0101, HLA-DRB1*0101) on a C57BL/6 background (HLA-DR1$^{+/+}$ I-Ab$^{-/-}$), a gift from Professor Danny Altmann, Imperial College London and C57BL/6 mice purchased from Charles River UK were used in influenza infection experiments. Mice were between 29 and 39 weeks of age at the time of infection and consisted of an unbiased ratio of male to female mice. Mice were housed in scantainers on a 12 h light/dark cycle, ventilated with HEPA filtered air and allowed access to standard mouse chow and water *ad libitum*. Mice were kept in specific pathogen-free conditions. All work was approved by the Animal Welfare and Ethical Review Board at Cardiff University and was carried out in accordance with the United Kingdom's Home Office and ARRIVE guidelines.

Viruses

IAVs used for infecting mice were the laboratory adapted strains A/Puerto Rico/8/34 (PR8, H1N1) and A/Aichi/2/68 (A/X31, H3N2); a reassortment virus expressing the H3 HA and N2 NA genes of A/Aichi/2/68 and the 6 internal genes of PR8.

Cell culture

Madin-Darby Canine Kidney (MDCK) cells (ATCC) and human embryonic kidney 293T (HEK293T or 293T) cells (ATCC) were maintained in Dulbecco's Modified Eagle Medium (DMEM) supplemented with 10% fetal bovine serum (FBS), 1% Non-Essential Amino Acids solution (NEAA), and 1% Penicillin-Streptomycin (Gibco). Both cell lines were maintained at 37°C, 5% CO_2.

Recombinant X31-HA-PKY virus

We generated the recombinant IAV named here as X31-HA-PKY using reverse genetics, a well-established technique to produce viable mutant viruses.[60] Modified HA was obtained by site-directed mutagenesis of pHW2000 plasmid containing the viral A/X31 HA sequence. The plasmid was sequenced to confirm the presence of the correct mutation. Virus was rescued using an 8-plasmid bidirectional reverse genetics system as previously described.[60] The eight plasmids were transfected into HEK293T cells using Lipofectamine and after overnight incubation transfected cells were co-cultured with MDCK cells cultured in serum-free DMEM supplemented with 1 μg/mL trypsin (Sigma-Aldrich). Virus was harvested 3 days after co-culture and stored at −80°C. Viral titer was determined by plaque assay as described below.

Mouse influenza infections

Female and male HLA-DR1 mice aged 29–39 weeks of age were infected intranasally under isoflurane anesthesia. Mice were infected with 200 pfu of A/X31, X31-HA-PKY or 50 pfu of PR8 in a total volume of 50 μL PBS. Mock infected mice received 50 μL of PBS under the same conditions. Bodyweight was recorded daily until sacrifice. If an animal lost >20% of bodyweight, they were sacrificed.

METHOD DETAILS

Viral plaque assays

Confluent monolayers of MDCK cells in 12-well plates were inoculated by serial 1:10 dilutions (10^{-1} to 10^{-6}) of 100 μL of IAV stocks or 10° to 10^{-5} dilutions of IAV infected mouse lung homogenate and incubated for 1 h at 37°C. The inoculum was removed, and cells overlaid with 1μg/ml trypsin in 2% agarose (Sigma-Aldrich) added to 10X MEM, 7.5% BSA, L-glutamine, 7.5% NaHCO3, penicillin/streptomycin (Gibco) 1M HEPES, 1% dextran (Sigma-Aldrich). Cells were incubated at 37°C and 5% CO_2. After 3 days, the agarose was removed, and the cells stained with crystal violet (1% crystal violet in methanol and water) and plaques enumerated.

Virus growth kinetics

Modified virus was analyzed for multicycle growth to confirm any effect of the mutation on viral replication *in vitro* compared with wild-type (parental) virus. MDCK cells were infected with either virus at a multiplicity of infection (MOI) of 0.01 and sampled at 16-, 24-, 48- and 72-h post infection. Virus yields were established by plaque assay.

Isolation of mouse tissue and cells

Splenocytes from naive and immune mice were collected from euthanised mice in RPMI 1640 with 10% FBS. For single cell splenocyte isolation, whole spleens were mashed through a 70 μM filter, centrifuged and pelleted cells washed in PBS. Cells were depleted of red blood cells by incubation with 1 × red blood cell lysis buffer on ice for 5 min. Splenocytes were centrifuged and washed in PBS and cells counted using the Novocyte 3000 flow cytometer (ACEA Biosciences). Single cell suspensions of splenocytes were used for ELISpot assay and flow cytometry.

Lungs were collected from euthanised mice in serum-free RPMI 1640 and snap-frozen in liquid nitrogen. Whole lungs were mashed with a tissue homogeniser and homogenates centrifuged at 3000 rpm for 10 min. Supernatants containing virus were assessed for viral titers by viral plaque assay as described above.

For flow cytometry analysis, lungs were collected from euthanised mice by severing the abdominal aorta. Lungs were perfused by injecting 5 mL of PBS in the left ventricle of the heart. Whole lungs were mechanically chopped and digested in collagenase at 2 mg/mL in a 37°C incushaker for 30 min. Lung tissue was washed in PBS, centrifuged, and pelleted cells resuspended in PBS for cell counting.

Peptides

15-mer peptides at >80% purity were synthesised commercially by GL.

Biochem, Shanghai or Peptide Protein Research, Hampshire. The following wild-type peptides were used: GLIYNRMGAVTTEVA, IDPFRLLQNSQVFSL, EDLIFLARSALILRG, PRMFLAMITYMTRNQ, VPDYASLRSLVASSG, APKYVKQNTLKLATG, SGPLKAEIAQR LEDV, RQMVQAMRTIGTHPS, MGMFNMLSTVLGVSI and PFR-modified peptides: GLIYNRMGAVTTE**R**A, IDPFRLLQNSQVF**R**L, ED LIFLARSALIL**A**G, PRMFLAMITYMTR**R**Q, VPDYASLRSLVAS**R**G, APKYVKQNTLKLA**R**G. Peptides were reconstituted in DMSO to a concentration of 20 mg/mL.

IFNγ ELISPOT assays

T cell responses to *ex vivo* restimulation with peptide was determined by IFN-γ enzyme-linked immunosorbent spot (ELISpot) assay as per manufacturer's instructions (Mabtech, Sweden). A total of 2.5 × 10^5 cells in RPMI 1640 with 10% heat treated FBS were added

per well of a 96-well ELISpot plate (MAIPS4510) pre-coated with anti-IFNγ capture antibody. Peptides were added at a final concentration of 5 μg/mL in duplicate wells for each peptide. Concanavalin A and media (without peptide) were used as positive and negative controls respectively. Plates were incubated at 37°C and 5% CO_2 for 18 h. The next day, plates were washed in PBS and incubated with mouse biotinylated anti-IFNγ (1:1000 in PBS) for 1 h at 37°C and 5% CO_2. Plates were washed in PBS and incubated with streptavidin-alkaline phosphatase for 1 h at room temperature before developing with 5-Bromo-4-chloro-3-indlylphospate/Nitroblue Tetrazolium (BCIT/NBP) chromogenic substrate for approximately 10 min in the dark. The reaction was stopped by rinsing plates in tap water. Plates were dried overnight and enumerated using the CTL Immunospot Analyser. The cut-off threshold for a positive response determined empirically and was at least double the background (value of SFC for no peptide control wells) and the mean of two duplicates greater than 12 SFC for 2.5 × 10^5 splenocytes as described before.[35]

Hemagglutination assay to titer influenza virus

Standardised amounts of A/X31 and PR8 viruses (measured in HA units) were determined by hemagglutination assay. An HA unit is defined as the amount of virus needed to agglutinate an equal volume of a standardised RBC suspension and is used in the assay to ensure the same amount of virus particles is used for each plate. Stock virus was 2-fold serially diluted and incubated with 0.5% turkey red blood cells in V bottomed 96-well plates for 1 h on ice. The assay titration endpoint, referred to as the last well where complete hemagglutination occurs, contains 1 HA unit. Because of the 2-fold serial dilutions used, two wells ahead of the titration endpoint corresponds to 4 HA units. Each virus is diluted accordingly to 4 HA units in PBS.

Hemagglutination inhibition (HI) assay

Sera from HLA-DR1 immune and naive mice were tested for influenza HI against A/X31 and PR8 viruses. Firstly, sera were treated (1:4) with receptor destroying enzyme (RDE; Denka Seiken, Tokyo, Japan) to remove non-specific inhibitors with an overnight incubation at 37°C followed by 1 h at 56°C. RDE-treated sera were then 2-fold serially diluted and incubated with standardised amount of virus (calculated as described above) for 15 min at room temperature and further incubated with the addition of 0.5% turkey red blood cells for 30 min at room temperature. Agglutination patterns were observed by tilting the plate. Non-agglutinated RBCs form a tear-like shape in the well and represent HA inhibition caused by blocking of virus agglutinating RBCs by virus-specific antibodies. The HI titer was calculated as the reciprocal of the last dilution of serum that completely inhibits hemagglutination.

Production of HLA-DR1 molecules

HLA-DR1 proteins for tetramer staining and crystallography were produced by *in vitro* refolding of HLA-DRα and HLA-DR1β chains from inclusion bodies produced in *Escherichia coli* as described previously.[35] For tetramer studies, the HLA-DRα chain was expressed with a C-terminal AviTag sequence to enable biotinylation. HLA-DR1 molecules were refolded in the presence of desired synthesised wild-type or modified peptides (GL Biochem). Refolded HLA-DR1 proteins were purified by affinity chromatography using the anti-HLA-DR clone L243 conjugated to a Pierce Protein G IgG Plus Orientation column (ThermoFisher Scientific) followed by size exclusion chromatography (Superdex S200 GL 10/300; Cytiva) using an AKTA Pure Fast Protein Liquid Chromatography (FPLC) system (Cytiva).

Assembly of pMHC-I and HLA-DR1 tetramers

H2-D^b restricted MHC-I monomers for $NP_{366-374}$, $PA_{224-233}$ and $PB1\text{-}F2_{62-70}$ epitopes were obtained from the NIH Tetramer Core Facility (Emory University, Atlanta). HLA-DR1 monomers refolded with DPF $NP_{301-315}$ and PKY $HA_{320-335}$ epitopes (or *P*11R variants) were made in house as above. Refolded HLA-DR1 monomers were biotinylated overnight at room temperature using a BirA biotin-protein ligase standard reaction kit (Avidity) prior to size exclusion chromatography to ensure removal of free biotin. Tetramers were assembled from pMHC-I and pMHC-II biotinylated monomers by conjugation to Streptavidin-PE (Biolegend). A total of 1 μg of each monomer were tetramerised per mouse. Streptavidin-PE was added in excess to biotinylated monomers at a ratio of 1.25:1 with a final concentration of 0.1 μg/μL of tetramer.

Tetramer staining

Lungs and spleens were harvested from mice and single cells isolated as described above. Cells were incubated with 100 nM protein kinase inhibitor (Dasatinib) at 37°C for 1 h (for pMHC-II tetramer) or PBS (for pMHC-I tetramer). Cells were stained with anti-CD16/32 antibody (Biolegend) (1:100) at 37°C for 10 min, for blocking non-specific binding of immunoglobulin to Fc receptors. 1 μg of pMHC tetramer-Streptavidin-PE was added to cells and incubated for 30 min at 37°C. Cells were then washed twice with PBS, stained with LIVE/DEAD Fixable Aqua Dead Cell Stain and incubated in the dark for 15 min. Cells were then washed twice with FACs buffer (2% FBS in PBS). For cell surface staining, cells were stained with pMHC-I tetramers or pMHC-II tetramers and α-CD3, α-CD4 and α-CD8, α-CD19, α-CD69, α-CD103 (Biolegend). Antibodies were incubated with cells at 4°C for 20 min. After incubation, cells were washed twice with FACs buffer and samples acquired directly on a Novocyte 3000 flow cytometer (ACEA Biosciences). Data were analyzed using Flow v10 (FlowJo, LLC).

Production of soluble F11 TCR

Soluble F11 TCR for crystallography was produced by *in vitro* refolding of F11-TCRα and F11-TCRβ chains from inclusion bodies produced in *Escherichia coli*[61] using the disulphide stabilised TRAC-TRBC domain construct described previously.[62] Soluble denatured inclusion bodies of TCR chains were refolded at a 1:1 ratio via rapid dilution into refold buffer (50 mM TRIS pH 8.1, 2 mM EDTA, 2.5 M urea, 0.74 g/L cysteamine & 0.83 g/L cystamine). Refold mixture was stirred vigorously at 4°C for 6 h before subsequent dialysis into 10 mM Tris pH 8.1. Refolded TCR was purified via anion exchange (POROS HQ50; ThermoFisher Scientific) and size exclusion (Superdex S200 GL 10/300; Cytiva) chromatography.

Crystallization and structure determination

For crystallisation trials, all proteins were eluted into 10 mM Tris pH 8.1, 10 mM NaCl during size exclusion chromatography. Samples of HLA-DR1-PKY (WT/*P*11R) were concentrated to ∼5 mg/mL following purification. For co-complex studies, F11 TCR and HLA-DR1-PKY-11R samples were mixed at a 1:1 M ratio and co-concentrated to ∼6 mg/mL. Crystallisation screening was performed using an Art Robbins Gryphon instrument, dispensing 400 nL drops of equal volume crystallisation solution and purified protein. All structures were derived from crystals obtained in conditions described in the TOPS screen[59]; HLA-DR1-PKY = 0.1 M HEPES pH 7.0, 25% PEG8000 &15% Glycerol; HLA-DR1-PKY-11R = 0.1 M MES pH 7.0, 25% PEG4000 & 0.2 M $(NH_4)_2SO_4$; F11-HLA-DR1-PKY-11R = 0.1 M Sodium cacodylate pH 6.515% PEG8000, 0.2 M $(NH_4)_2SO_4$.

Crystals tested for diffraction were cryoprotected in mother liquor solution supplemented with 10% ethylene glycol. Crystals were harvested from drops using mounted LithoLoops (Molecular Dimensions), snap frozen in liquid nitrogen and exposed to X-rays at Diamond Light Source (Harwell Campus, UK). Data were processed using *xia2*[63] which implements *DIALS*,[64] *XDS*,[65] *POINTLESS*[66] & *AIMLESS*.[67] Phases were estimated via molecular replacement in *PHASER*[68] using appropriate components of the F11-HLA-DR1-PKY structure as search ensembles.[35] Peptide atoms were omitted from search models to prevent model bias. Structures were refined via iterative rounds of refinement in *PHENIX*[69] and manual model building in COOT v0.9.6,[70] assessing progression of model quality with MolProbity.[71] TLS groups for TLS refinement were determined using *phenix.find_tls_groups.* For omit map analysis, a two macro-cycle refinement of *phenix.refine* that included simulated annealing was performed in the absence of specified omitted atoms and subsequent electron density maps generated using *phenix.mtz2map*. TCR crossing angle calculations were performed as was described by *Rudolph et al.*[46] All images were generated using an open-source build of PyMOL v2.5 (Schrödinger, LLC.). Co-ordinates and structure factors were submitted to the PDB under the accession codes: HLA-DR1-PKY = 8PJE, HLA-DR1-hPKY-11R = 8PJF & F11-HLA-DR1-PKY-11R = 8PJG.

QUANTIFICATION AND STATISTICAL ANALYSIS

Statistical analysis & flow cytometry analysis

Statistical tests were performed using Prism 10 (GraphPad Software). The statistical test used for each experiment is indicated in the figure legend. Analysis of flow cytometry data was performed using FlowJo 10. Cells were gated on the following parameters: lymphocytes/single cells/live cells/$CD3^+$ cells. Cells were then gated on either $CD4^+$ or $CD8^+$. $CD4^+$ and $CD8^+$ cells were gated with markers CD69 and CD103, or $H2\text{-}D^b$ and HLA-DR1 tetramers.